Peridynamics for Bending of Beams and Plates with Transverse Shear Deformation

C. Diyaroglu*, E. Oterkus*, S. Oterkus and E. Madenci****
* Department of Naval Architecture, Ocean and Marine Engineering
University of Strathclyde, Glasgow, United Kingdom

** Department of Aerospace and Mechanical Engineering
University of Arizona, Tucson, United States of America

Progressive failure analysis of structures is still a major challenge. There exist various predictive techniques to tackle this challenge by using both classical (local) and nonlocal theories. Peridynamic (PD) theory (nonlocal) is very suitable for this challenge, but computationally costly with respect to the finite element method. When analyzing complex structures, it is necessary to utilize structural idealizations to make the computations feasible. Therefore, this study presents the PD equations of motions for structural idealizations as beams and plates while accounting for transverse shear deformation. Also, their PD dispersion relations are presented and compared with those of classical theory.

1. Introduction

Peridynamic (PD) theory was originally introduced for the solution of deformation field equations (Silling, 2000) without any structural idealizations. It satisfies all the fundamental balance laws of classical (local) continuum mechanics; however, it is different in the sense that it is a nonlocal continuum theory and it introduces an internal length parameter into the field equations. This internal length parameter defines the association among the material points within a finite distance through micropotentials. Removal of micropotentials between the material points allows damage initiation and growth through a single critical failure parameter regardless of the mixed-mode loading conditions. The creation of a new (crack) surface is based on a local damage measure. The local damage is defined as the ratio of broken interactions to the total number of interactions at a material point.

Finite Element Analysis (FEA) with traditional elements suffers from the following shortcomings: (1) The interface between dissimilar materials is assumed to have zero thickness without any specific material properties; however, it presents a weak link and it is usually the location of failure. Therefore, it fails to appropriately model the interface between dissimilar materials. (2) Failure is a dynamic process, and it requires remeshing. It is computationally costly, and the crack growth is guided based on the linear elastic fracture mechanics (LEFM) concepts. It breaks down when multiple complex crack growth patterns develop. (3) Stress and strain fields are discontinuous, and mesh refinement does not necessarily ensure accurate stress fields near geometric and material discontinuities. (4) Finally, crack nucleation is not resolved. The analysis always requires a pre-existing crack.

Keywords: Peridynamics, Timoshenko Beam, Mindlin Plate, Transverse Shear Deformation, Dispersion Relationships

In order to remedy or remove these shortcomings, Cohesive Zone Elements (CZE) and eXtended Finite Elements (XFEM) were developed; however, CZE requires a priori knowledge of the crack path. In a complex analysis, it is not practical and the results are dependent on the mesh (structured or unstructured). Furthermore, the results are sensitive to the strength parameters in the traction-separation law of the cohesive zone model. Determination of these parameters poses additional uncertainties. Although XFEM removed such uncertainties, it still requires an external criteria for crack propagation. Thus, the results depend on the criteria employed in the analysis. It also breaks down when multiple complex crack growth patterns develop.

The PD theory overcomes the weaknesses of the existing methods, and it is capable of identifying all of the failure modes without simplifying assumptions. The PD methodology effectively predicts complex failure in complex structures under general loading conditions. Damage is inherently calculated in a PD analysis without special procedures, making progressive failure analysis more practical.

An extensive literature survey on PD is given in a recently published textbook by Madenci and Oterkus (2014). A comparison study between peridynamics, CZE, and XFEM techniques is given by Agwai et al. (2011). They showed that the crack speeds obtained from all three approaches are on the same order; however, the fracture paths obtained by using peridynamics are closer to experimental results with respect to other two techniques.

Another advantage of PD is its length-scale parameter, which does not exist in classical continuum mechanics. Such a length-scale parameter gives PD a nonlocal character. Hence, it allows the capture of physical phenomena not only at the macro-scale, but also at various other scales. This characteristic can be established through the PD dispersion relations. The classical theory is only valid for a special case of a long wavelength limit; however, the PD shows dispersion behavior similar to that observed in real materials. Hence, it is proven to be acceptable to perform multi-scale analysis simulations.

Although peridynamics is a powerful technique in failure analysis and has an internal length scale, it is usually computationally more expensive, especially with respect to finite element analysis. The computational time can be significantly reduced by using parallel computing either by using a CPU (Central Processing Unit) and/or GPU - based (Graphics Processing Unit) architecture for which PD equations of motion are very suitable. However, modeling very large and detailed structures such as aerospace and marine vehicles can still be computationally demanding. Hence, in such cases it is necessary to reduce computational time through structural idealization. Taylor and Steigmann (2013) proposed a peridynamic plate model based on bond-based formulation by using an asymptotic analysis. The formulation is capable of capturing out-of-plane deformations for thin plates. Moreover, O'Grady and Foster (2014a,b) developed a non-ordinary state-based peridynamic model for Euler-Bernoulli beam and Kirchhoff-Love plate formulations by disregarding the transverse shear deformations. Therefore, the focus of this study is present a new PD formulation for thin or thick beams and plates by taking into account transverse shear deformation, i.e. a Timoshenko beam and Mindlin plate, respectively, based on an original (bond-based) PD formulation. Moreover, PD dispersion relations are obtained and compared against those from classical theory.

The following sections present the PD kinematics for a Timoshenko beam and a Mindlin plate, and the corresponding PD equations of motion as well as the PD material parameters. They also describe the procedure to determine the surface correction factors for these parameters and the application of the boundary conditions and determination of the critical curvature and critical shear angle in terms of the fracture mechanics parameters. Finally, the corresponding dispersion relations are derived and compared with the classical theory. The numerical results establish the validity of the present formulation by considering simple benchmark problems.

2. Peridynamic kinematics

At any instant of time, every point in the beam or plate denotes the out-of-plane deflection and rotations of a material particle, and these infinitely many material points (particles) constitute the beam or the plate. In the undeformed state of the body, each material point is identified by its coordinates, $\mathbf{x}_{(k)}$ with $(k = 1, 2, ..., \infty)$, and is associated with an incremental volume, $V_{(k)}$, and a mass density of $\rho(\mathbf{x}_{(k)})$. According to the PD theory introduced by Silling (2000), the motion of a body is analyzed by considering the pair-wise interaction between material points $\mathbf{x}_{(k)}$ and $\mathbf{x}_{(j)}$. The interaction between the material points is prescribed through a micropotential that depends on the deformation and constitutive properties of the material. Also, a material point is only influenced by the other material points within a neighborhood defined by its horizon, δ. The micropotentials are zero for material points outside its horizon. Each material point can be subjected to prescribed body loads, displacement, or velocity, resulting in motion and deformation.

2.1. Beam kinematics

As shown in Fig. 1, the transverse shear angles, $\varphi_{(j)}$ and $\varphi_{(k)}$, of material points j and k can be expressed as

$$\varphi_{(j)} = \left(\frac{w_{(j)} - w_{(k)}}{\xi_{(j)(k)}} - \phi_{(j)} \operatorname{sgn}\left(x_{(j)} - x_{(k)}\right) \right) \tag{1a}$$

$$\varphi_{(k)} = \left(\frac{w_{(j)} - w_{(k)}}{\xi_{(j)(k)}} - \phi_{(k)} \operatorname{sgn}\left(x_{(j)} - x_{(k)}\right) \right) \tag{1b}$$

in which $w_{(j)}$, $\phi_{(j)}$ and $w_{(k)}$, $\phi_{(k)}$ represent the out-of-plane deflection and rotation of material points j and k, respectively. The distance between the material points j and k is specified as $\xi_{(j)(k)} = \left| x_{(j)} - x_{(k)} \right|$.

Considering the material point k as the point of interest, the transverse shear angle, $\varphi_{(k)(j)}$, arising from the interaction between material points j and k can be defined as the average of the transverse shear angles at these material points in the form

$$\varphi_{(k)(j)} = \left(\frac{w_{(j)} - w_{(k)}}{\xi_{(j)(k)}} - \frac{\phi_{(j)} + \phi_{(k)}}{2} \operatorname{sgn}\left(x_{(j)} - x_{(k)} \right) \right) \tag{2}$$

The curvature between the material points j and k can be defined as

$$\kappa_{(k)(j)} = \left(\frac{\phi_{(j)} - \phi_{(k)}}{\xi_{(j)(k)}} \right) \tag{3}$$

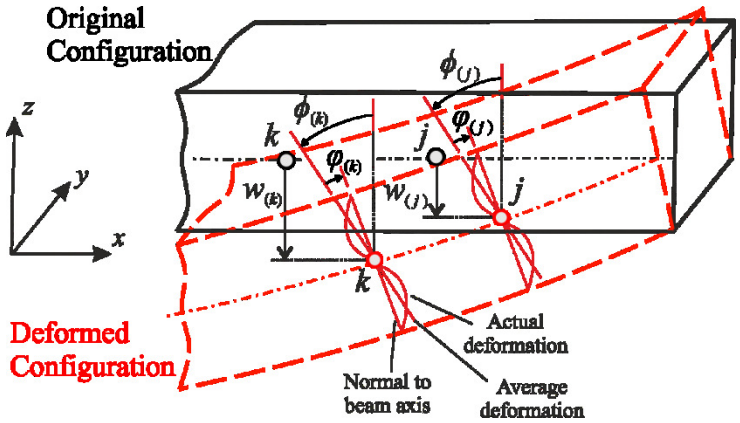

Figure 1. Original and deformed configurations of a Timoshenko beam.

When considering the material point j as the point of interest, the transverse shear angle and curvature for the interaction between the material points j and k become

$$\varphi_{(j)(k)} = \left(\frac{w_{(k)} - w_{(j)}}{\xi_{(j)(k)}} - \left(-\frac{\phi_{(k)} + \phi_{(j)}}{2} \right) \operatorname{sgn}\left(x_{(j)} - x_{(k)} \right) \right) \quad \text{or} \quad \varphi_{(j)(k)} = -\varphi_{(k)(j)} \tag{4a}$$

and

$$\kappa_{(j)(k)} = \left(\frac{\phi_{(k)} - \phi_{(j)}}{\xi_{(j)(k)}} \right) \quad \text{or} \quad \kappa_{(j)(k)} = -\kappa_{(k)(j)} \tag{4b}$$

2.2. Plate kinematics

As illustrated in Fig. 2, $\phi_{(j)}$ and $\phi_{(k)}$ represent the rotations with respect to the line of action between the material points j and k. Considering the material point k as the point of interest, the curvature, $\kappa_{(k)(j)}$, with respect to the line of action between the material points j and k can be defined as

$$\kappa_{(k)(j)} = \frac{\phi_{(j)} - \phi_{(k)}}{\xi_{(j)(k)}} \tag{5}$$

Through coordinate transformation, the rotations and curvature with respect to the line of action between the material points j and k can be decomposed as

$$\phi_{(j)} = \phi_{x(j)} \cos\theta + \phi_{y(j)} \sin\theta \tag{6a}$$

$$\phi_{(k)} = \phi_{x(k)} \cos\theta + \phi_{y(k)} \sin\theta \tag{6b}$$

and

$$\kappa_{(k)(j)} = \left(\frac{\phi_{x(j)} - \phi_{x(k)}}{x_{(j)} - x_{(k)}} \right) \cos^2\theta + \left(\frac{\phi_{y(j)} - \phi_{y(k)}}{y_{(j)} - y_{(k)}} \right) \sin^2\theta \tag{7}$$

in which $x_{(j)} - x_{(k)} = \xi_{(j)(k)} \cos\theta$ and $y_{(j)} - y_{(k)} = \xi_{(j)(k)} \sin\theta$, with $\xi_{(j)(k)}$ representing the distance between material points j and k. The slope with respect to the line of action between the material points j and k can be expressed as

$$\vartheta_{(k)(j)} = \frac{w_{(j)} - w_{(k)}}{\xi_{(j)(k)}} \tag{8}$$

in which $w_{(j)}$ and $w_{(k)}$ represent the out-of-plane deflections at material points j and k. As sketched in Fig. 2, the transverse shear angles at material points j and k can be expressed as

$$\varphi_{(j)} = \vartheta_{(k)(j)} - \phi_{(j)} \tag{9a}$$

$$\varphi_{(k)} = \vartheta_{(k)(j)} - \phi_{(k)} \tag{9b}$$

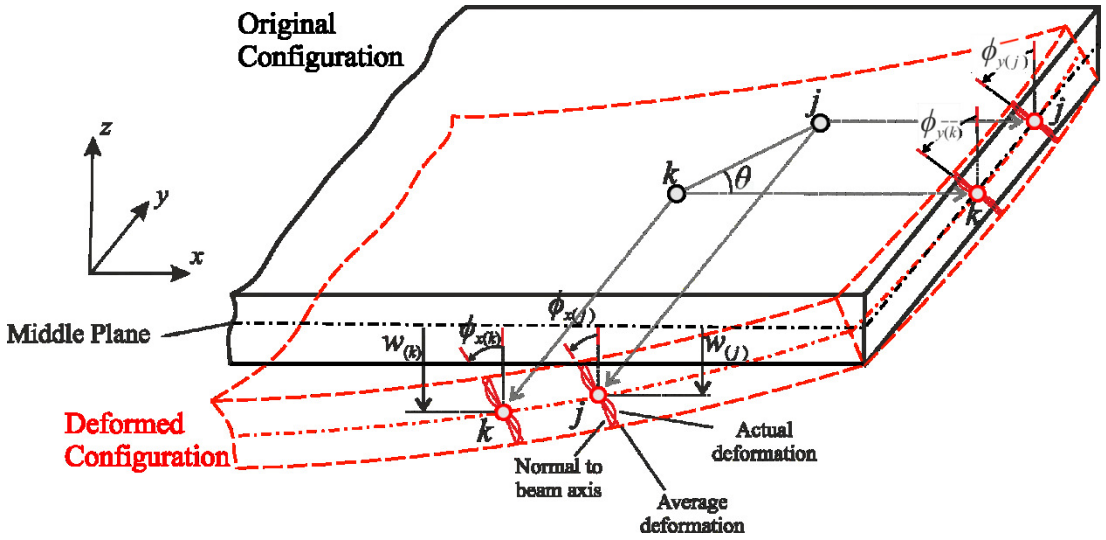

Figure 2. Original and deformed configurations of a Mindlin plate.

Considering the material point k as the point of interest, the transverse shear angle, $\varphi_{(k)(j)}$, between material points j and k can be defined as the average of the shear angles at these material points in the form

$$\varphi_{(k)(j)} = \frac{w_{(j)} - w_{(k)}}{\xi_{(j)(k)}} - \frac{\phi_{(j)} + \phi_{(k)}}{2} \tag{10a}$$

or

$$\varphi_{(k)(j)} = \frac{w_{(j)} - w_{(k)}}{\xi_{(j)(k)}} - \frac{\left(\phi_{x(j)}\cos\theta + \phi_{y(j)}\sin\theta\right) + \left(\phi_{x(k)}\cos\theta + \phi_{y(k)}\sin\theta\right)}{2} \tag{10b}$$

When considering the material point j as the point of interest, the transverse shear angle and curvature for the interaction between the material points j and k become

$$\varphi_{(j)(k)} = \frac{w_{(k)} - w_{(j)}}{\xi_{(j)(k)}} - \left(-\frac{\phi_{(k)} + \phi_{(j)}}{2}\right) \tag{11a}$$

and

$$\kappa_{(j)(k)} = \frac{\phi_{(k)} - \phi_{(j)}}{\xi_{(j)(k)}} \tag{11b}$$

It is worth noting that $\varphi_{(j)(k)} = -\varphi_{(k)(j)}$ and $\kappa_{(j)(k)} = -\kappa_{(k)(j)}$.

3. Peridynamic equations of motion

The PD equations of motion at material point k can be derived by applying the principle of virtual work

$$\delta\int_{t_0}^{t_1}(T-U)dt=0 \tag{12}$$

where T and U represent the total kinetic and potential energies in the beam or plate. This principle is satisfied by solving for the Lagrange equation

$$\frac{d}{dt}\left(\frac{\partial L}{\partial \dot{\mathbf{q}}_{(k)}}\right)-\frac{\partial L}{\partial \mathbf{q}_{(k)}}=0\,, \tag{13}$$

where the vector $\mathbf{q}_{(k)}$ includes the independent field variables (out-of-plane deflection and rotations), and the Lagrangian L is defined as

$$L=T-U\,. \tag{14}$$

3.1. Beam equations of motion

The total kinetic energy of the system due to bending and transverse shear deformation can be written as

$$T=\frac{1}{2}\sum_{k=1}^{\infty}\rho\left[\dot{w}_{(k)}+\frac{I}{A}\left(\dot{\phi}_{(k)}\right)\right]V_{(k)} \tag{15}$$

in which $V_{(k)}$ represents the infinitesimally small incremental volume of material point k and the dot (.) above a parameter denotes differentiation with respect to time. The parameters ρ, I, and A correspond to mass density of the material, the moment of inertia, and the cross sectional area of the beam, respectively.

The total potential energy of the system can be obtained by summing the micropotentials, $\tilde{w}_{(k)(j)}(\varphi_{(k)(j)})$ and $\hat{w}_{(k)(j)}(\varphi_{(k)(j)})$, between material points arising from bending and transverse shear deformation

$$\begin{aligned}U=&\sum_{k=1}^{\infty}\left\{\frac{1}{2}\sum_{j=1}^{\infty}\frac{1}{2}\left[\tilde{w}_{(k)(j)}\left(\varphi_{(k)(j)}\right)+\tilde{w}_{(j)(k)}\left(\varphi_{(j)(k)}\right)\right]V_{(j)}-\tilde{b}_{(k)}w_{(k)}\right\}V_{(k)}\\&+\sum_{k=1}^{\infty}\left\{\frac{1}{2}\sum_{j=1}^{\infty}\frac{1}{2}\left[\hat{w}_{(k)(j)}\left(\varphi_{(k)(j)}\right)+\hat{w}_{(j)(k)}\left(\varphi_{(j)(k)}\right)\right]V_{(j)}-\hat{b}_{(k)}w_{(k)}\right\}V_{(k)}\end{aligned} \tag{16}$$

in which $\tilde{\iota}_{(k)}$ and $\hat{b}_{(k)}$ represent the body moment and body force at material point k. The independent variables are out-of-plane deflection and rotation of the material point, $w_{(k)}$ and $\phi_{(k)}$. Hence, the resulting Euler-Lagrange equations can be expressed as

$$\frac{d}{dt}\frac{\partial L}{\partial \dot{w}_{(k)}} - \frac{\partial L}{\partial w_{(k)}} = 0 \tag{17a}$$

and

$$\frac{d}{dt}\frac{\partial L}{\partial \dot{\phi}_{(k)}} - \frac{\partial L}{\partial \phi_{(k)}} = 0 \tag{17b}$$

Using the Lagrangian definition $L = T - U$ and performing differentiation yield the following equations of motion

$$\rho \ddot{w}_{(k)} - \sum_{j=1}^{\infty} \frac{1}{2}\left[\xi_{(j)(k)} \hat{f}_{(k)(j)} \frac{\partial \varphi_{(k)(j)}}{\partial\left(w_{(k)}\right)} + \xi_{(j)(k)} \hat{f}_{(j)(k)} \frac{\partial \varphi_{(j)(k)}}{\partial\left(w_{(k)}\right)} \right] V_{(j)} - \hat{b}_{(k)} = 0 \tag{18a}$$

and

$$\begin{aligned} \frac{\rho I}{A} \ddot{\phi}_{(k)} - \sum_{j=1}^{\infty} \frac{1}{2} \xi_{(j)(k)} \Bigg[& \tilde{f}_{(k)(j)} \frac{\partial\left(\kappa_{(k)(j)}\right)}{\partial\left(\phi_{(k)}\right)} + \tilde{f}_{(j)(k)} \frac{\partial\left(\kappa_{(j)(k)}\right)}{\partial\left(\phi_{(k)}\right)} \Bigg] V_{(j)} \\ & + \sum_{j=1}^{\infty} \frac{1}{2} \xi_{(j)(k)} \left[\hat{f}_{(k)(j)} \frac{\partial \varphi_{(k)(j)}}{\partial\left(\phi_{(k)}\right)} + \hat{f}_{(j)(k)} \frac{\partial \varphi_{(j)(k)}}{\partial\left(\phi_{(k)}\right)} \right] V_{(j)} - \tilde{\iota}_{(k)} = 0 \end{aligned} \tag{18b}$$

in which $\hat{f}_{(k)(j)}$, $\hat{f}_{(j)(k)}$, $\tilde{f}_{(k)(j)}$, and $\tilde{f}_{(j)(k)}$ are defined as

$$\hat{f}_{(k)(j)} = \frac{1}{\xi_{(j)(k)}} \frac{\partial \hat{w}_{(k)(j)}\left(\varphi_{(k)(j)}\right)}{\partial \varphi_{(k)(j)}} \quad , \quad \hat{f}_{(j)(k)} = \frac{1}{\xi_{(j)(k)}} \frac{\partial \hat{w}_{(j)(k)}\left(\varphi_{(j)(k)}\right)}{\partial \varphi_{(j)(k)}} \tag{19a,b}$$

and

$$\tilde{f}_{(k)(j)} = \frac{1}{\xi_{(j)(k)}} \frac{\partial \tilde{w}}{\partial\left(\kappa_{(k)(j)}\right)} \quad , \quad \tilde{f}_{(j)(k)} = \frac{1}{\xi_{(j)(k)}} \frac{\partial \tilde{w}}{\partial\left(\kappa_{(j)(k)}\right)} \tag{20a,b}$$

They represent the peridynamic interaction forces between material points j and k arising from transverse shear deformation and bending. For a linear material behavior, they can also be defined in the form

$$\hat{f}_{(k)(j)} = c_s\left(\varphi_{(k)(j)}\right) \quad \text{and} \quad \hat{f}_{(j)(k)} = c_s\left(\varphi_{(j)(k)}\right) \tag{21a,b}$$

and

$$\tilde{f}_{(k)(j)} \quad c_b \left(\varphi_{(k)(j)}\right) \quad \cdots\cdots \quad \tilde{f}_{(j)(k)} \quad c_b \left(\varphi_{(j)(k)}\right) \tag{22a,b}$$

in which c_s and c_b are the peridynamic material parameters associated with the transverse shear deformation and bending of the beam, respectively.

Invoking Eqs. (2-4) and substituting for the peridynamic forces from Eqs. (21) and (22) in Eq. (18) result in

$$\rho \ddot{\quad} \sum_{j=1}^{\infty}\left(\frac{w_{(j)} - w_{(k)}}{\xi_{(j)(k)}} - \frac{\phi_{(j)} + \phi_{(k)}}{2}\operatorname{sgn}\left(x_{(j)} - x_{(k)}\right)\right) V_{(j)} + \hat{b}_{(k)} \tag{23a}$$

and

$$\frac{\rho I}{A} \ddot{\quad} \quad \sum_{j=1}^{\infty} \frac{\phi_{(j)} - \phi_{(k)}}{\xi_{(j)(k)}} V_{(j)} + \frac{1}{2} c_s \sum_{j=1}^{\infty}\left(\frac{w_{(j)} - w_{(k)}}{\xi_{(j)(k)}}\operatorname{sgn}\left(x_{(j)} - x_{(k)}\right) - \frac{\phi_{(j)} + \phi_{(k)}}{2}\right) \xi_{(j)(k)} V_{(j)} + \tilde{\iota}_{(k)} \tag{23b}$$

As mentioned earlier, if the peridynamic interactions are limited within the horizon, then these equations can also be written in an integral form as

$$\rho \ddot{\quad} \quad c_s \int_H \left(\frac{w(x',t) - w(x,t)}{\xi} - \frac{\phi(x',t) + \phi(x,t)}{2}\operatorname{sgn}\left(x' - x\right)\right) dV' + \hat{b}(x,t) \tag{24a}$$

and

$$\begin{aligned} \frac{\rho I}{A} \ddot{\quad} \quad & \int_H \left(c_b \frac{\phi(x',t) - \phi(x,t)}{\xi}\right) dV' \\ & + \int_H \left(\frac{1}{2} c_s \left(\frac{w(x',t) - w(x,t)}{\xi}\operatorname{sgn}\left(x' - x\right) - \frac{\phi(x',t) + \phi(x,t)}{2}\right)\xi\right) dV' + \tilde{\iota} \end{aligned} \tag{24b}$$

As derived in Appendix A, the PD material constants c_s and c_b can be expressed in terms of the shear and Young's moduli, G and E, as

$$c_s = \frac{2kG}{A\delta^2} \quad \text{and} \quad c_b = \frac{2EI}{\delta^2 A^2} + \frac{1}{4}\frac{kG}{A} \tag{25a,b}$$

in which k is the shear correction factor, and is equal to $5/6$ for rectangular cross sections.

3.2. Plate equations of motion

The total kinetic energy of the system due to bending and transverse shear deformation can be expressed as

$$T = \frac{1}{2}\rho\sum_{k=1}^{\infty}\Big[\dot{\quad}_{(k)} \quad \dot{\quad}_{(k)} \quad \dot{\quad}_{(k)}\Big] A_{(k)} \tag{26}$$

Invoking the representation of the in-plane displacement components in terms of rotations as $u_{(k)} = -z\phi_{x(k)}$ and $v_{(k)} = -z\phi_{y(k)}$ and performing integration through the thickness of the plate result in

$$T = \frac{1}{2}\rho\sum_{k=1}^{\infty}\left(\int_{-h/2}^{h/2}\Big[\dot{\quad}_{(k)} \quad \dot{\quad}_{(k)} \quad \dot{\quad}_{(k)}\Big] dz\right) A_{(k)} \tag{27a}$$

or

$$T = \frac{1}{2}h\rho\sum_{k=1}^{\infty}\left(\dot{\quad}_{(k)} \quad \frac{h^2}{12}\dot{\quad}_{(k)} \quad \frac{h^2}{12}\dot{\quad}_{(k)}\right) A_{(k)} \tag{27b}$$

in which $A_{(k)}$ represents the infinitesimally small incremental area of each material point and h represents the thickness of the plate.

The total potential energy of the plate can be obtained by summing the micropotentials, $\tilde{w}_{(k)(j)}\left(\quad_{(k)(j)}\right)$ and $\hat{w}_{(k)(j)}\left(\varphi_{(k)(j)}\right)$, between material points arising from bending and transverse shear deformation

$$\begin{aligned} U = &\sum_{k=1}^{\infty}\left\{\frac{1}{2}\sum_{j=1}^{\infty}\frac{1}{2}\Big[\tilde{w}_{(k)(j)}\left(\quad_{(k)(j)}\right) \quad \tilde{w}_{(j)(k)}\left(\quad_{(j)(k)}\right)\Big] V_{(j)} - \frac{\tilde{\iota}_{\alpha(k)}}{h}\phi_{\alpha(k)}\right\} V_{(k)} \\ &+\sum_{k=1}^{\infty}\left\{\frac{1}{2}\sum_{j=1}^{\infty}\frac{1}{2}\Big[\hat{w}_{(k)(j)}\left(\varphi_{(k)(j)}\right)+\hat{w}_{(j)(k)}\left(\varphi_{(j)(k)}\right)\Big] V_{(j)} - \frac{\hat{b}_{(k)}}{h}w_{(k)}\right\} V_{(k)} \end{aligned} \tag{28}$$

in which $\tilde{\iota}_{\alpha(k)}$ and $\hat{b}_{(k)}$ represent the resultant body moment and body force at material point k. The independent variables are out-of-plane deflection and rotations of the material point, $w_{(k)}$ and $\phi_{\alpha(k)}$. Hence, the resulting Euler-Lagrange equations can be expressed as

$$\frac{d}{dt}\frac{\partial L}{\partial \dot{w}_{(k)}} - \frac{\partial L}{\partial w_{(k)}} = 0 \tag{29a}$$

and

$$\frac{d}{dt}\frac{\partial L}{\partial \dot{\phi}_{\alpha(k)}} - \frac{\partial L}{\partial \phi_{\alpha(k)}} = 0 \quad \text{with} \quad \alpha = x, y \tag{29b}$$

Using the Lagrangian definition $L = T - U$, performing the differentiation while invoking Eqs. (6, 7) and (10, 11), and substituting from Eqs. (19-22) yield the following equations of motion

$$\rho h \ddot{w}_{(k)} = \sum_{j=1}^{\infty}\left(\frac{w_{(j)} - w_{(k)}}{\xi_{(j)(k)}} - \frac{\phi_{x(j)} + \phi_{x(k)}}{2}\cos\theta - \frac{\phi_{y(j)} + \phi_{y(k)}}{2}\sin\theta\right) V_{(j)} + \hat{b}_{(k)} \tag{30a}$$

$$\begin{aligned}\rho\frac{h^3}{12}\ddot{\phi}_{x(k)} &= \sum_{j=1}^{\infty}\left[\left(\frac{\phi_{x(j)} - \phi_{x(k)}}{\xi_{(j)(k)}}\right)\cos\theta + \left(\frac{\phi_{y(j)} - \phi_{y(k)}}{\xi_{(j)(k)}}\right)\sin\theta\right]\cos\theta\, V_{(j)} \\ &+ \frac{1}{2}c_s\sum_{j=1}^{\infty}\xi_{(j)(k)}\left(\frac{w_{(j)} - w_{(k)}}{\xi_{(j)(k)}} - \frac{\phi_{x(j)} + \phi_{x(k)}}{2}\cos\theta - \frac{\phi_{y(j)} + \phi_{y(k)}}{2}\sin\theta\right)\cos\theta\, V_{(j)} + \tilde{\iota}_{x(k)}\end{aligned} \tag{30b}$$

and

$$\begin{aligned}\rho\frac{h^3}{12}\ddot{\phi}_{y(k)} &= \sum_{j=1}^{\infty}\left[\left(\frac{\phi_{x(j)} - \phi_{x(k)}}{\xi_{(j)(k)}}\right)\cos\theta + \left(\frac{\phi_{y(j)} - \phi_{y(k)}}{\xi_{(j)(k)}}\right)\sin\theta\right]\sin\theta\, V_{(j)} \\ &+ \frac{1}{2}c_s\sum_{j=1}^{\infty}\xi_{(j)(k)}\left(\frac{w_{(j)} - w_{(k)}}{\xi_{(j)(k)}} - \frac{\phi_{x(j)} + \phi_{x(k)}}{2}\cos\theta - \frac{\phi_{y(j)} + \phi_{y(k)}}{2}\sin\theta\right)\sin\theta\, V_{(j)} + \tilde{\iota}_{y(k)}\end{aligned} \tag{30c}$$

Note that the peridynamic interactions are limited within the horizon of material points. As derived in Appendix A, the PD material constants c_s and c_b can be expressed in terms of the shear and Young's moduli, G and E, as

$$c_s = \frac{9E}{4\pi\delta^3}k^2 \quad \text{and} \quad c_b = \frac{E}{\pi\delta}\left(\frac{3h^2}{4\delta^2} + \frac{27}{80}k^2\right) \tag{31a,b}$$

in which k^2 is the shear correction factor that can be chosen based on the frequency of the lowest thickness shear mode as $k^2 = \pi^2/12$, and $\nu = 1/3$.

The PD material parameters c_b and c_s are determined for a material point whose horizon is completely embedded in the material. For these material points, both classical and peridynamic

Strain Energy Densities (SED) are equivalent. However, the PD material parameters c_b and c_s require correction if the material point is close to boundaries. The correction of the material parameters is achieved by numerically integrating the SED at each material point inside the body for simple loading conditions and comparing them to their counterparts obtained from classical solutions. SED is composed of bending and transverse shear deformation. Therefore, the parameter c_b is corrected by $\bar{g}_b$ based on the SED due to the bending, and c_s by $\bar{g}_s$ due to the transverse shear deformation. Their derivation is explicitly described in Appendix B.

4. Boundary conditions

Unlike the local theory, the boundary conditions are imposed through a nonzero volume of fictitious boundary layers. This necessity arises because the PD field equations do not contain any spatial derivatives; therefore, constraint conditions are, in general, not necessary for the solution of an integro-differential equation. However, such conditions can be imposed by prescribing constraints through a fictitious boundary layer.

In order to apply a displacement or rotation constraint, a fictitious boundary layer, R_c, is introduced outside the actual material, as shown in Fig. 3. The size of this layer is equivalent to the horizon. An external load, such as a moment or a transverse load, can be applied in the form of body loads through a layer within the actual material, R_ℓ. This layer can have a thickness of a single layer of material points if the discretization is done by using a meshless approach (Madenci and Oterkus, 2014).

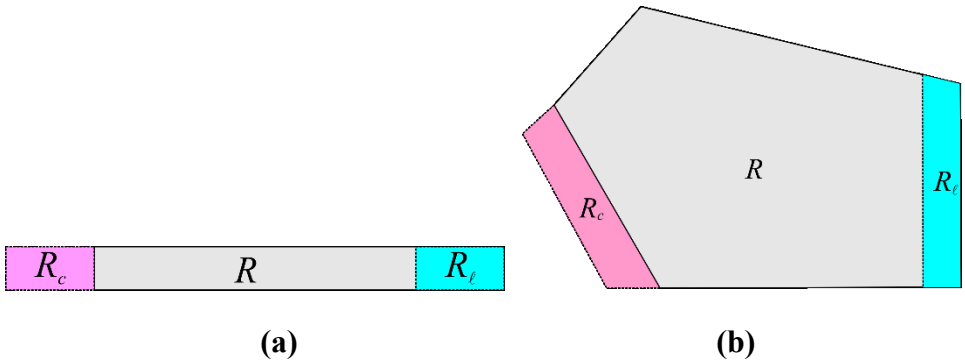

Figure 3. Application of boundary conditions in peridynamics: (a) beam and (b) plate.

5. Peridynamic dispersion relations

Peridynamic dispersion relations are compared against those of the classical Timoshenko and Mindlin plate theories. In the derivation of these dispersion relations, the wave number, the wave frequency and phase velocity of the wave are denoted by κ, ω, and υ, respectively. The relationship among these parameters is $\omega = \kappa\upsilon$. The compressional and shear wave speeds are defined by $\upsilon_c^2 = E/\rho$ and $\upsilon_s^2 = G/\rho$, respectively, where G and E are the shear and Young's

moduli of the material. The wave number is related to the half-wavelength, Γ, by the relationship $\kappa = \pi/\Gamma$.

5.1 Beam dispersion relations

Dispersion relations are determined by considering a wave propagating in the *x*-direction. Therefore, wave solutions for material points located at x and x' can be expressed as

$$w(x,t) = w_0 e^{i(\kappa x - \omega t)} \text{ and } w(x',t) = w_0 e^{i(\kappa x - \omega t + \mathrm{sgn}(x'-x)\kappa\xi)} \tag{32a}$$

$$\phi(x,t) = \phi_0 e^{i(\kappa x - \omega t)} \text{ and } \phi(x',t) = \phi_0 e^{i(\kappa x - \omega t + \mathrm{sgn}(x'-x)\kappa\xi)} \tag{32b}$$

in which $\kappa\xi$ is the phase difference between material points located at x and x', and ϕ_0 and w_0 represent the amplitudes of these waves.

Substituting these wave solutions into the PD equations of motion given in Eq. (24) leads to a homogeneous set of equations for ϕ_0 and w_0. For a nontrivial solution to exist, the determinant of their coefficient matrix must vanish, resulting in the wave dispersion relation as

$$\begin{vmatrix} 2Ac_s B_2 - \rho\omega^2 & Ac_s B_3 \\ -Ac_s B_3 & 2Ac_b B_2 + \frac{1}{2} Ac_s B_1 - \rho \frac{I}{A}\omega^2 \end{vmatrix} = 0 \tag{33}$$

where the terms B_i with $i = 1,2,3$ are explicitly given in Appendix C; they are dependent on the phase difference and the horizon. As explained in Appendix C, for long wavelength (or small wave number, κ), the resulting wave dispersion relation is the same as that of the classical theory (Reis, 1978; Amirkulova, 2011). As expected, both theories yield the same relationship for long wavelength.

For specified values of $E = 200$ GPa, $\rho = 7850$ kg/m^3, $k = 5/6$, $h = 10^{-7}$ m, $\nu = 0.3$, and finite horizon size, $\delta = 10^{-8}$ m, the evaluation of the determinant without any simplification leads to the variation of the wave frequency, ω, as a function of the wave number, κ, for the first and second modes as shown in Fig. 4. Although both modes involve a combination of transverse and angular displacements, the first mode is dominated by transverse motion and the second mode is dominated by angular motion (Reis, 1978). For both modes, the PD wave dispersions level off as the wave number increases which is a well-known behavior observed in experimental studies (Eringen, 1972; Weckner and Silling, 2011). However, the wave frequency always increases linearly according to the classical theory (CT).

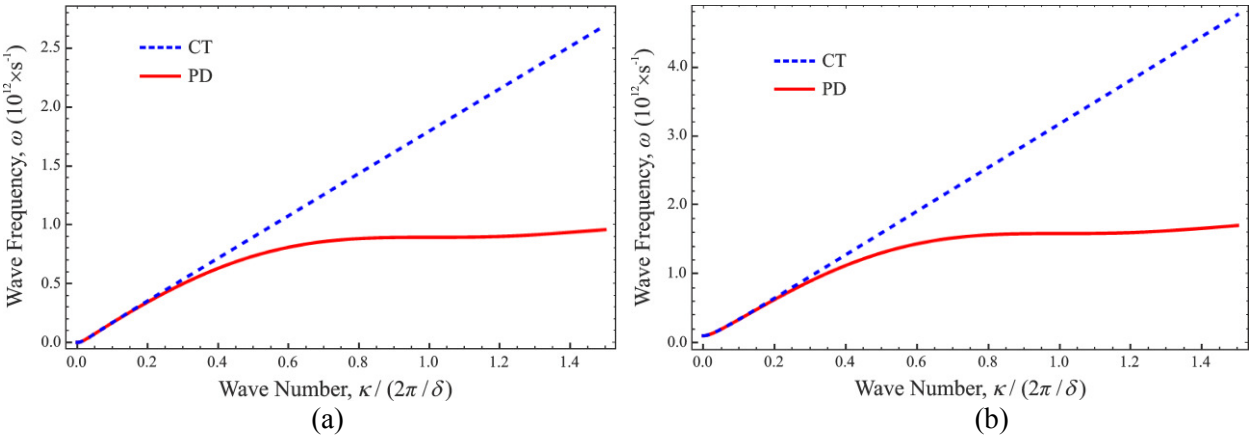

Figure 4. Comparison of PD and CT wave frequency dispersions: (a) first mode and (b) second mode.

The variation of the normalized phase speed, $\upsilon/\left(\upsilon_s\sqrt{k}\right)$ as a function of wave number, κ, for the first mode is shown in Fig. 5a. As shown in Fig. 5a, both PD and CT predict zero speed in the limit as κ approaches zero. The phase speed of the CT reaches a constant value close to the shear wave speed of a bar for short wavelengths (or relatively large wave numbers). For the second mode, both theories predict comparable results for the long wavelengths (or relatively small wave numbers) while classical phase speed reaches the compressional wave speed, υ_c, of a bar for short wavelengths (or relatively large wave numbers), as depicted in Fig. 5b. However, the phase speed decreases as the wave number increases according to the PD theory as observed in real materials.

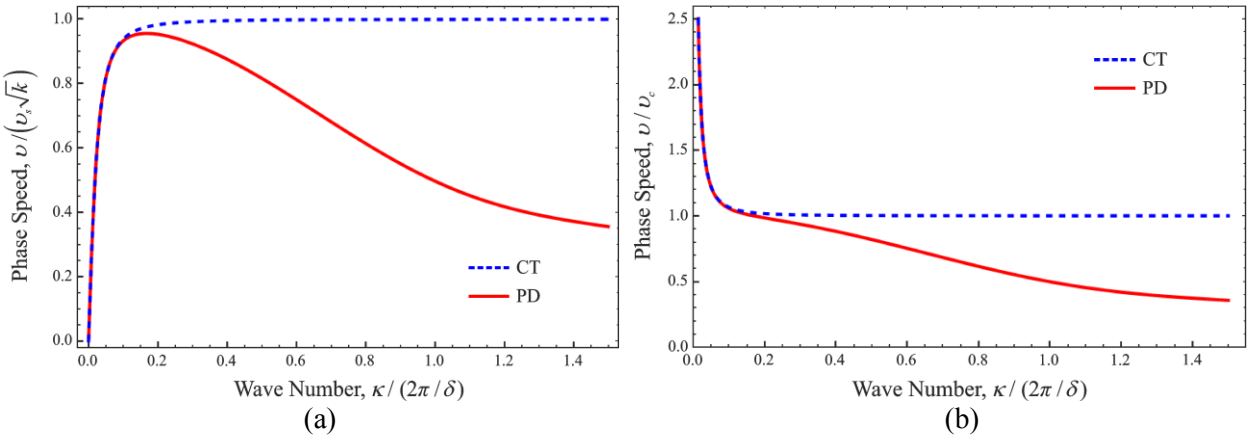

Figure 5. Comparison of PD and CT wave speed dispersions: (a) first mode and (b) second mode.

5.2. Plate dispersion relations

As in the case of a beam, the dispersion relations for a plate can be obtained by considering a wave propagating in the *x*-direction. Therefore, wave solutions for material points located at x and x' can be expressed as

$$w(\mathbf{x},t)=w_0e^{i(\kappa x-\omega t)} \text{ and } w(\mathbf{x}',t)=w_0e^{i(\kappa x-\omega t+\kappa\xi\cos(\theta))} \tag{34a}$$

$$\phi_x(\mathbf{x},t)=\phi_{x0}e^{i(\kappa x-\omega t)} \text{ and } \phi_x(\mathbf{x}',t)=\phi_{x0}e^{i(\kappa x-\omega t+\kappa\xi\cos(\theta))} \tag{34b}$$

$$\phi_y(\mathbf{x},t)=\phi_{y0}e^{i(\kappa x-\omega t)} \text{ and } \phi_y(\mathbf{x}',t)=\phi_{y0}e^{i(\kappa x-\omega t+\kappa\xi\cos(\theta))} \tag{34c}$$

in which $\kappa\xi\cos(\theta)$ is the phase difference between material points located at x and x', and w_0, ϕ_{x0} and ϕ_{y0} represent the amplitudes of these waves.

Substituting these wave solutions into the PD equations of motion given in Eq. (30) leads to a homogeneous set of equations for ϕ_{x0}, ϕ_{y0}, and w_0. For a nontrivial solution to exist, the determinant of their coefficient matrix must vanish, resulting in the wave dispersion relation as

$$\begin{vmatrix} c_sM_1+\rho h\omega^2 & -c_sM_2 & -c_sM_3 \\ \frac{1}{2}c_sM_6 & c_bM_4-\frac{1}{2}c_sM_7+\frac{\rho h^3}{12}\omega^2 & c_bM_5-\frac{1}{2}c_sM_8 \\ \frac{1}{2}c_sM_{10} & c_bM_5-\frac{1}{2}c_sM_8 & c_bM_9-\frac{1}{2}c_sM_{11}+\frac{\rho h^3}{12}\omega^2 \end{vmatrix}=0 \tag{35}$$

where the terms M_i with $i=1,.....,11$ are explicitly given in Appendix C; they are dependent on the phase difference and the horizon. As explained in Appendix C, for long wavelength (or small wave number, κ), the resulting wave dispersion relation is the same as that of the CT (Soedel, 2004). Thus, both theories give the same relationship for long wavelength.

For specified values of $E=200$ GPa, $\rho=7850$ kg/m^3, $h=5\times10^{-8}$ m, $k^2=5/(6-\nu)$, $\nu=1/3$, and finite horizon size, $\delta=10^{-8}$m, the evaluation of the determinant without any simplifications leads to the variation of the wave frequency, ω, as a function of the wave number, κ. Figure 6 shows comparisons of nondimensionalized phase speed $(\upsilon/(\upsilon_s\sqrt{k^2}))$ as a function of wave number $\kappa/(2\pi/\delta)$ for the first three modes; lowest flexural mode ω_1, thickness-shear mode ω_2, and thickness-twist mode ω_3.

As observed in Fig. 6a, both the classical and PD theories estimate zero speed in the limit as wave number, κ, approaches zero, whereas the classical theory phase speed nearly approaches the Rayleigh surface wave speed, $\upsilon/\upsilon_s=0.9274$, for Poisson's ratio of $\nu=0.30$ as wave number, κ, increases (Stephen, 1997). In Figs. 6b and 6c, both theories estimate comparable results for the long wavelengths (or relatively small κ). However, PD theory captures the feature of real materials that phase velocity decreases as the wave number increases. Also comparisons of wave frequency dispersions for increasing wave number are shown in Fig. 7. As a characteristic of real materials, dispersion curves of the peridynamic theory for all modes level

off as the wave number increases and exceeds a value of $2\pi/\delta$ (Silling, 2000). Thus, PD theory captures the experimentally observed feature of real materials, which are always dispersive as a result of long-range forces.

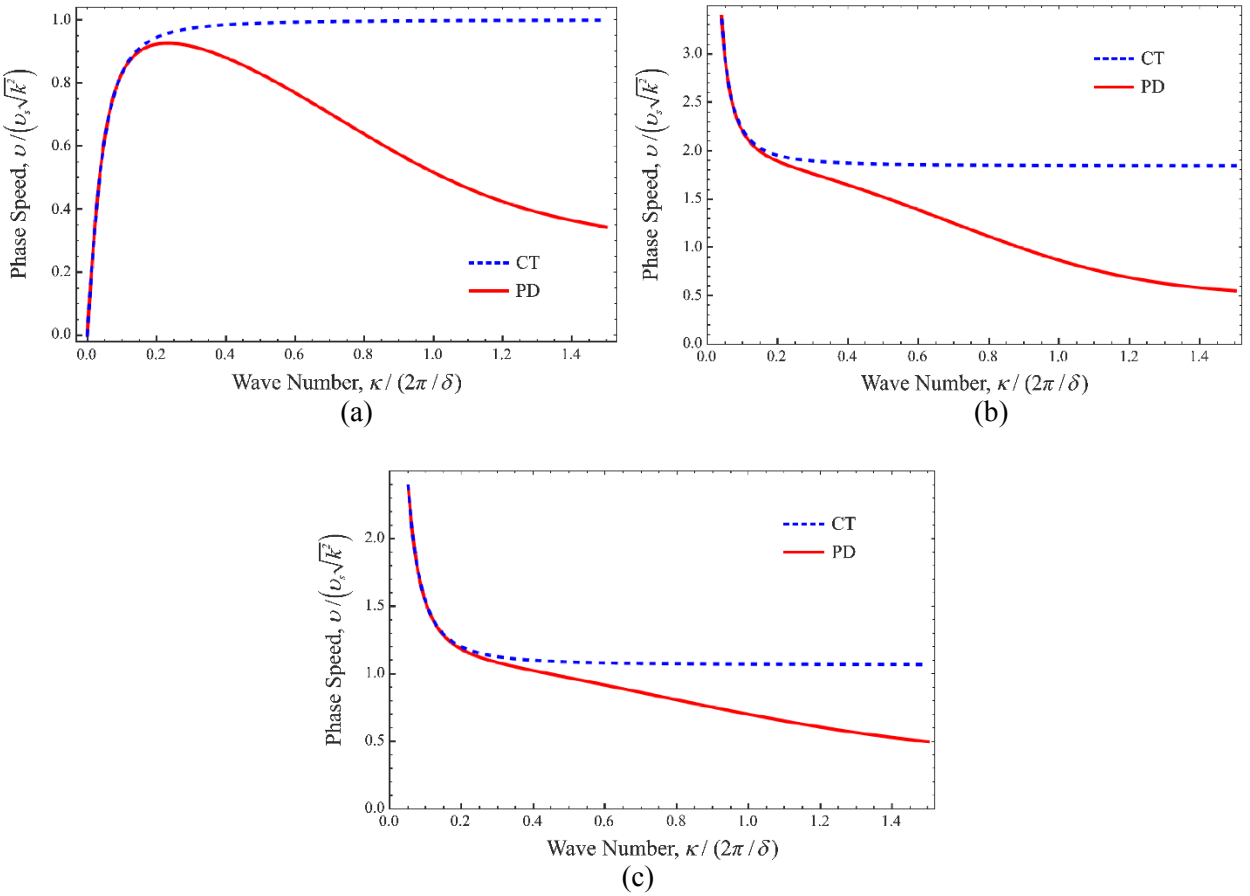

Figure 6. Comparison of wave speed dispersions: (a) lowest flexural mode ω_1, (b) thickness-shear mode ω_2, and (c) thickness-twist mode ω_3.

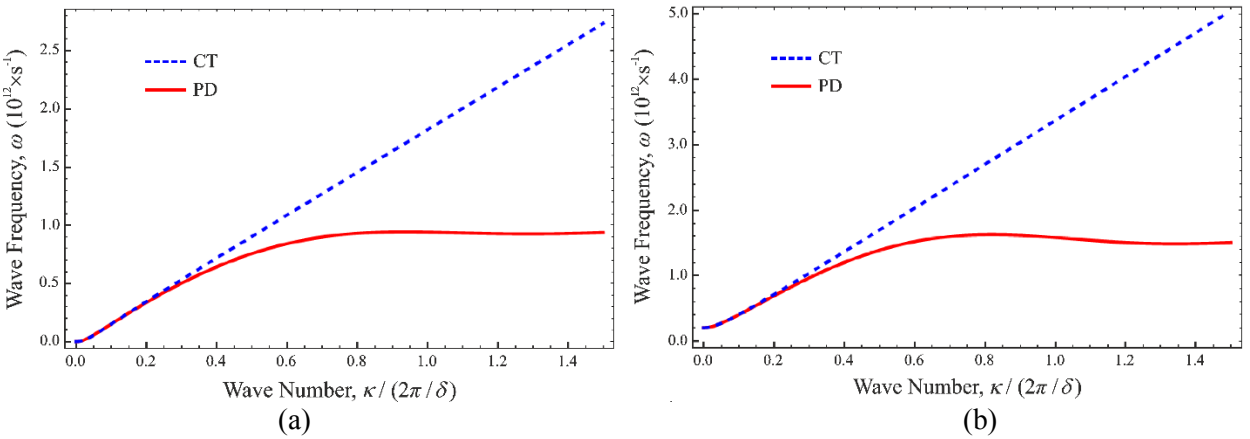

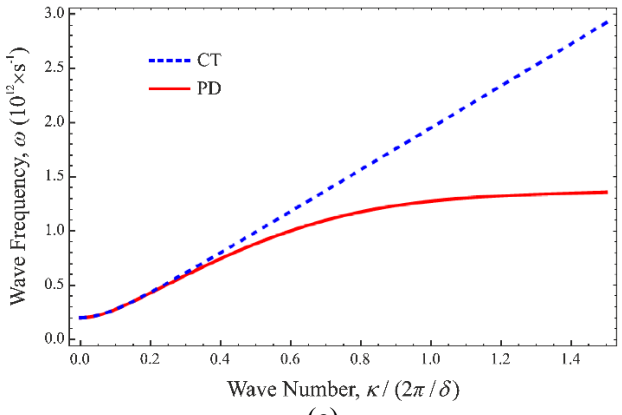

(c)

Figure 7. Comparison of wave frequency dispersions: (a) lowest flexural mode ω_1, (b) thickness-shear mode ω_2, and (c) thickness-twist mode, ω_3

6. Critical curvature and critical angle

In order to include failure in the material response, the response functions in the governing equations for the plate can be modified through a history-dependent scalar value function, $H(x_{(j)}-x_{(k)},t)$ as

$$\hat{f}_{(k)(j)} = c_s H\left(x_{(j)}-x_{(k)},t\right)\left(\varphi_{(k)(j)}\right) \tag{36a}$$

and

$$\tilde{f}_{(k)(j)} = c_b H\left(x_{(j)}-x_{(k)},t\right)\left(\kappa_{(k)(j)}\right) \tag{36b}$$

It is defined as

$$H\left(x_{(j)}-x_{(k)},t\right)=\begin{cases}1 & \text{if } \left|\kappa_{(k)(j)}\left(x_{(j)}-x_{(k)},t'\right)\right|<\kappa_c \text{ and } \left|\varphi_{(k)(j)}\left(x_{(j)}-x_{(k)},t'\right)\right|<\varphi_c \\ 0 & \text{otherwise}\end{cases} \tag{37}$$

Critical curvature and angle values can be expressed in terms of the critical energy release rate of the material. In order to find these relationships, the total strain energy required to remove all of the interactions across a newly created crack surface, A, shown in Fig. 8, must be determined and equated to the corresponding critical energy release rate value.

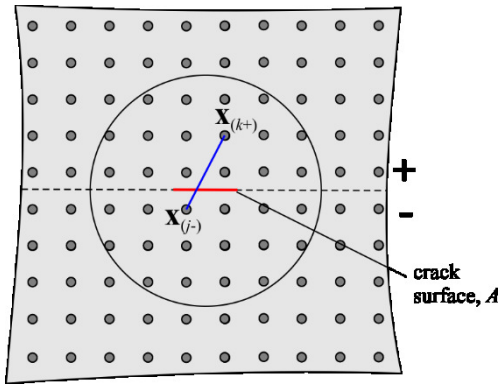

Figure 8. Interaction between two material points whose line of action crosses the crack surface.

The total bending strain energy required to remove all of the interactions across the new crack surface A is

$$W_b^c = \sum_{k=1}^{K^+}\sum_{j=1}^{J^-}\frac{1}{2}c_b\left(\kappa_c\right)^2\left(\left|\mathbf{x}_{(j^-)}-\mathbf{x}_{(k^+)}\right|\right)V_{(k^+)}V_{(j^-)} \tag{38}$$

The total bending strain energy, W_b^c, can be equated to the mode-I critical energy release rate, G_{Ic}, in order to determine the value of the bending critical curvature as

$$G_{Ic} = \frac{\frac{1}{2}c_b\left(\kappa_c\right)^2\sum_{k=1}^{K^+}\sum_{j=1}^{J^-}\left(\left|\mathbf{x}_{(j^-)}-\mathbf{x}_{(k^+)}\right|\right)V_{(k^+)}V_{(j^-)}}{A} \tag{39}$$

Based on the expression derived by Silling and Askari (2005) and Madenci and Oterkus (2013) for the critical energy release rate, it is evident that

$$\frac{\sum_{k=1}^{K^+}\sum_{j=1}^{J^-}\left(\left|\mathbf{x}_{(j^-)}-\mathbf{x}_{(k^+)}\right|\right)V_{(k^+)}V_{(j^-)}}{A} = \frac{h\delta^4}{2} \tag{40}$$

Finally, the critical curvature can be expressed as

$$\kappa_c = \sqrt{\frac{4G_{Ic}}{c_b h\delta^4}} \tag{41}$$

Similarly, the total shear strain energy required to remove all of the interactions across the surface A is

$$W_s^c = \sum_{k=1}^{K^+}\sum_{j=1}^{J^-}\frac{1}{2}c_s\left(\varphi_c\right)^2\left(\left|\mathbf{x}_{(j^-)}-\mathbf{x}_{(k^+)}\right|\right)V_{(k^+)}V_{(j^-)} \tag{42}$$

This total shear strain energy, W_s^c, can be equated to the mode-III critical energy release rate, G_{IIIc}, in order to determine the value of the critical shear angle as

$$G_{IIIc} = \frac{\frac{1}{2} c_s \left(\varphi_c\right)^2 \sum_{k=1}^{K^+} \sum_{j=1}^{J^-} \left(\left| \mathbf{x}_{(j^-)} - \mathbf{x}_{(k^+)} \right| \right) V_{(k^+)} V_{(j^-)}}{A} \tag{43}$$

By using the relationship given in Eq. (40), the critical shear angle can be obtained as

$$\varphi_c = \sqrt{\frac{4G_{IIIc}}{c_s h \delta^4}} \tag{44}$$

7. Results

As part of the numerical results, simple static loading conditions are considered first to compare the PD predictions with the analytical solutions. A plate with a center crack under bending is considered next. In order to obtain the static solution, the adaptive dynamic relaxation technique given by Kilic and Madenci (2010) is used, and the horizon size is chosen as $\delta = 3.015\Delta x$ where Δx is the uniform grid spacing.

7.1. Timoshenko beam subjected to pure bending and transverse loading

The length of the beam is $L = 1\text{m}$, with a cross sectional area of $A = 0.1 \times 0.1\text{m}^2$. Its Young's modulus is specified as $E = 200\,\text{GPa}$. Only a single row of material (collocation) points are necessary to discretize the beam. The distance between material points is $\Delta x = 0.01\text{m}$. The left edge is constrained by introducing a fictitious region with a size of δ. The beam is first subjected to bending moment and then transverse loading, as shown in Figs. 9 and 10. The loading is applied to a single material point at the right end of the bar as a body load of $\tilde{b}$ [illegible] $10^9\ \text{N/m}^2$ for bending and $\hat{b} = 5 \times 10^9\ \text{N/m}^3$ for the transverse loading, corresponding to an applied moment of $M = 3.33 \times 10^5\ \text{Nm}$ and a transverse load of $P = 5 \times 10^5\ \text{N}$, respectively.

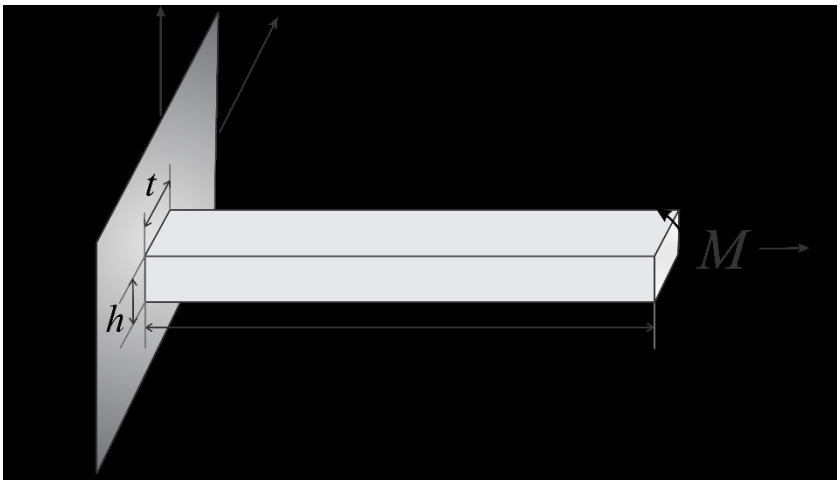

(a)

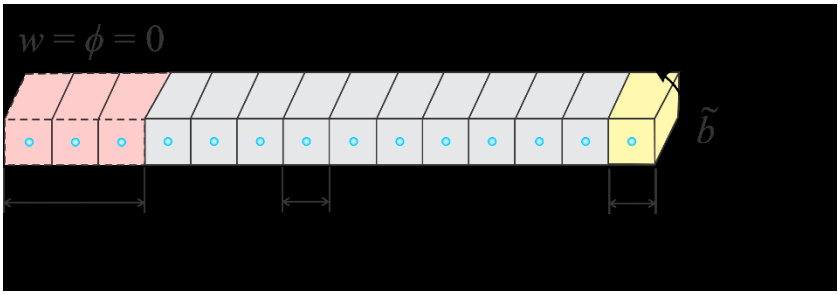

(b)

Figure 9. (a) Timoshenko beam subjected to pure bending and (b) its discretization.

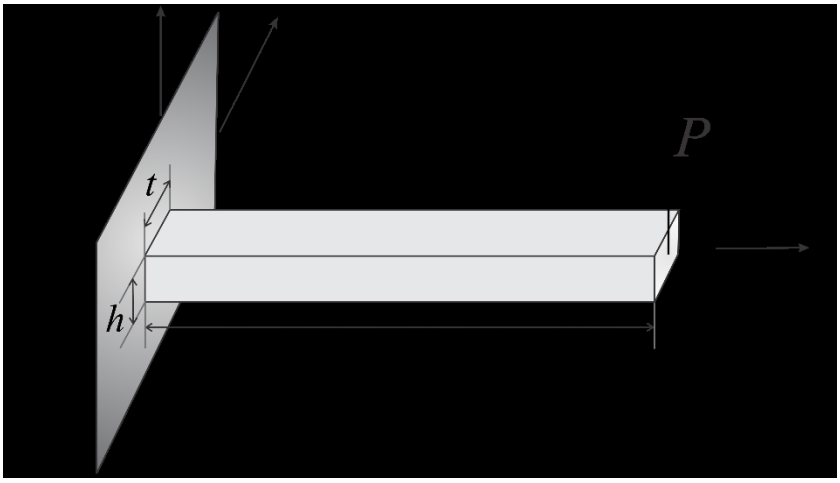

(a)

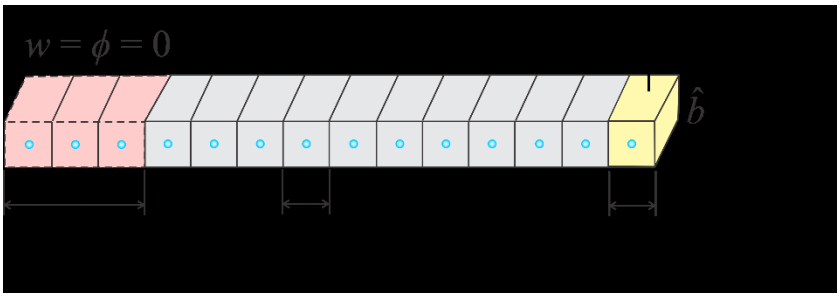

(b)

Figure 10. (a) Timoshenko beam subjected to transverse loading and (b) its discretization.

The analytical solutions for the transverse displacement and the rotation due to pure bending are given as

$$w = \frac{Mx^2}{2EI} \tag{45a}$$

and

$$\phi = \frac{Mx}{EI} \tag{45b}$$

As depicted in Fig. 11, the PD and analytical solutions are in good agreement.

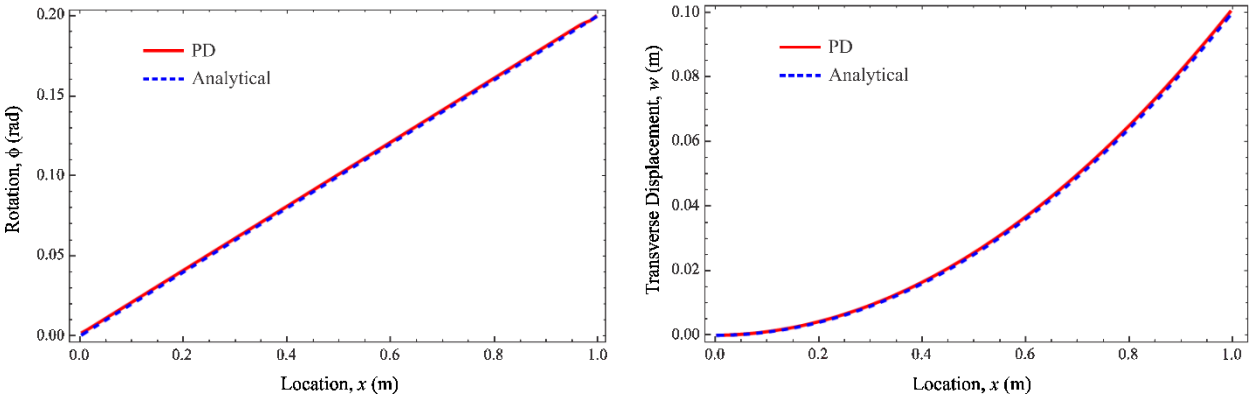

(a) **(b)**

Figure 11. Variation of (a) rotation and (b) transverse displacement along a Timoshenko beam subjected to pure bending loading.

Under the transverse loading case, the analytical solutions for the transverse displacement and the rotation are given as

$$w = \frac{Px}{kGA} + \frac{P}{2EI}\left(Lx^2 - \frac{x^3}{3}\right) \tag{46a}$$

and

$$\phi = \frac{P\left(2Lx - x^2\right)}{2EI} \tag{46b}$$

As shown in Fig. 12, the PD and the analytical solutions also agree well with each other. This verifies that the PD equations of motion accurately captures the deformation behavior of a Timoshenko beam.

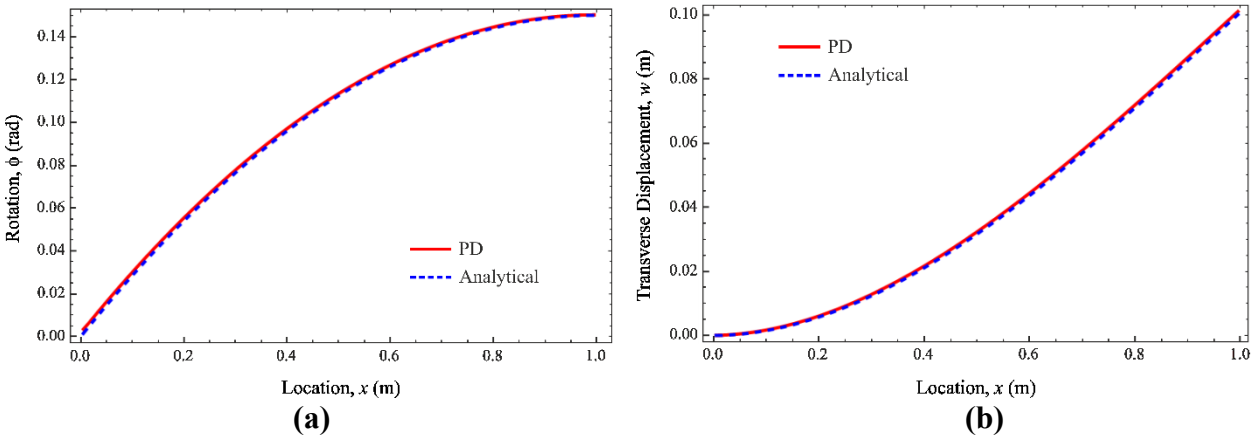

Figure 12. Variation of (a) rotation and (b) transverse displacement along a Timoshenko beam subjected to transverse force loading.

7.2. Mindlin plate subjected to pure bending and transverse force loading

As shown in Figs. 13 and 14, the length and width of the plate is $L = W = 1\,\text{m}$ with a thickness of $h = 0.1\,\text{m}$. The Young's modulus of the plate is specified as $E = 200\,\text{GPa}$. Only a single row of material (collocation) points in the thickness direction is necessary to discretize the domain. The distance between material points is $\Delta x = 0.01\,\text{m}$. The left edge is constrained by introducing a fictitious region with a size of $3\Delta x$. The loading is applied to a single row of material points at the right end of the plate as a resultant body load of $\tilde{\iota}_x$ [illegible] $10^8\,\text{N/m}$ for bending and $\hat{b} = 5\times10^8\,\text{N/m}^2$ for the transverse loading.

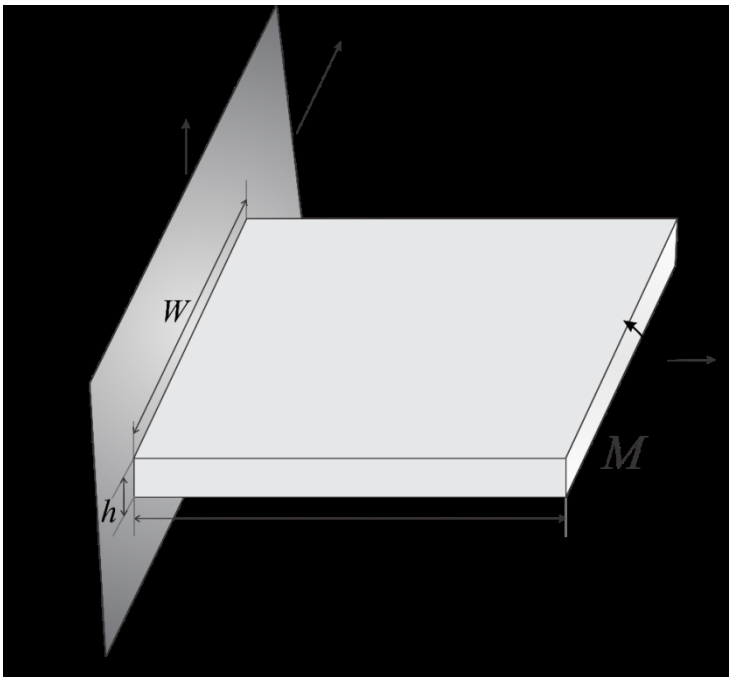

(a)

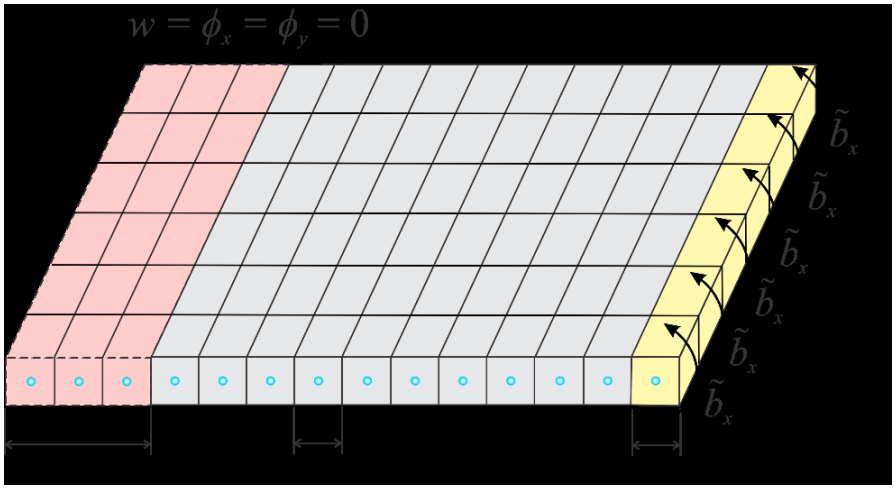

(b)

Figure 13. (a) Mindlin plate subjected to pure bending loading and (b) its discretization.

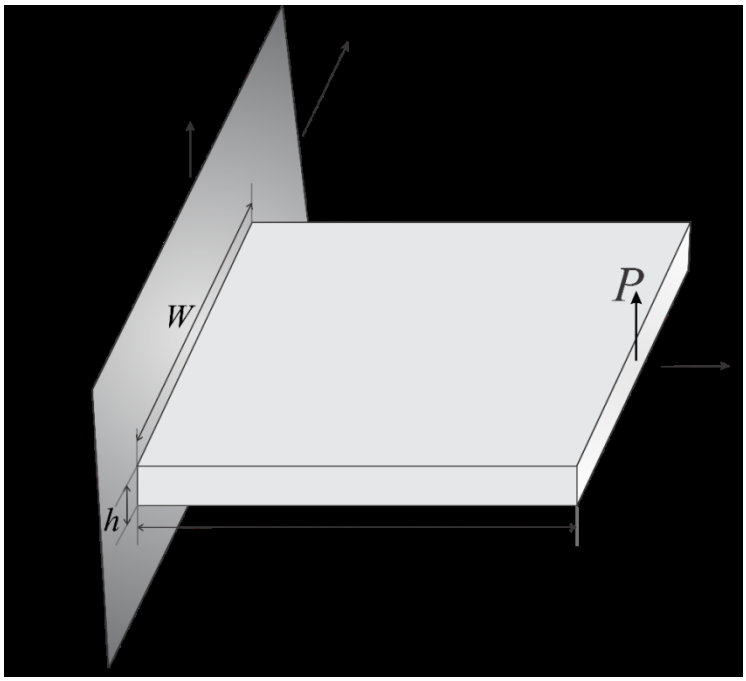

(a)

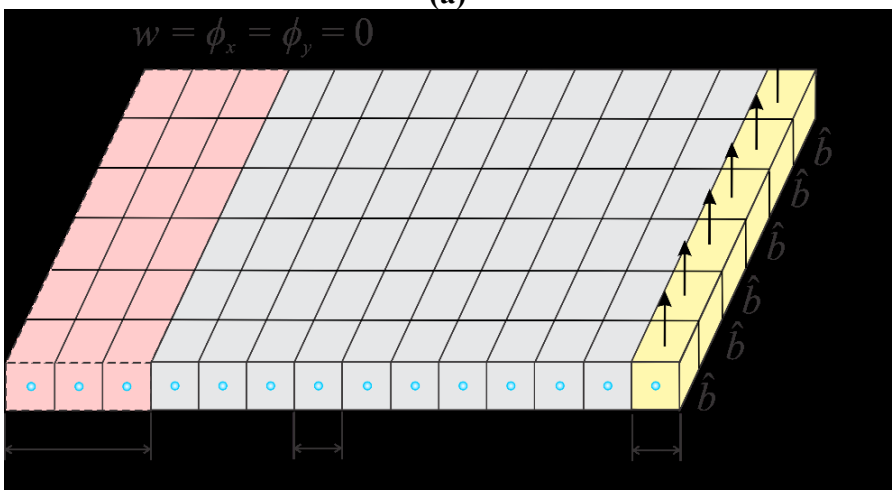

(b)

Figure 14. (a) Mindlin plate subjected to transverse force loading and (b) its discretization.

The peridynamic solutions of the transverse displacement and the x-direction rotation for bending moment and transverse loading cases are compared with finite element (FE) solutions by using a shell element, which is suitable for thick shell structures, available in commercial software, ANSYS.

As depicted in Figs. 15 and 16, the PD and the FE solutions agree well with each other. This verifies that the PD equation of motion given in Eqs. (30a-c) can accurately capture the deformation behavior of a Mindlin plate.

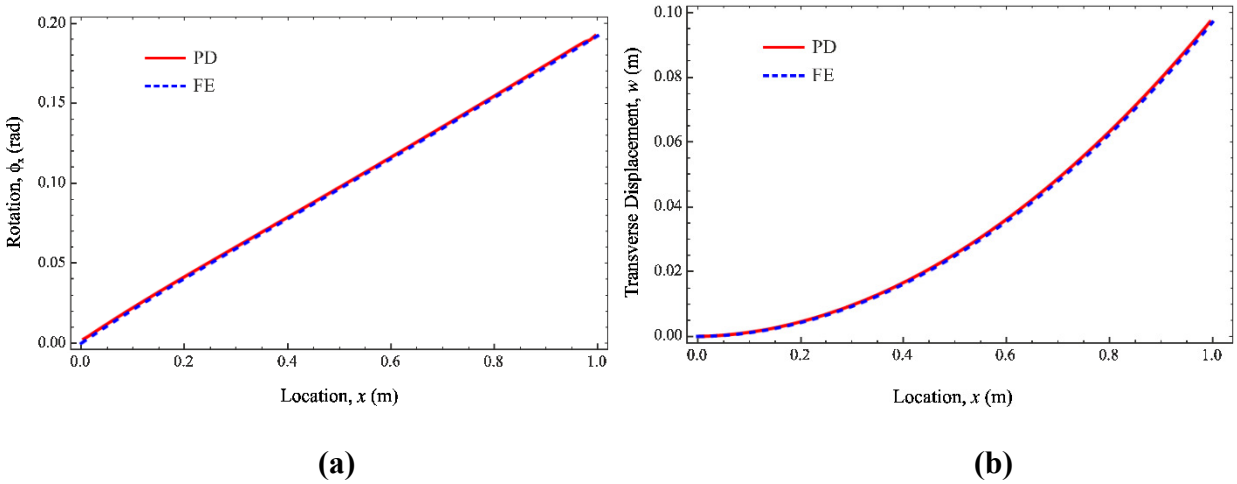

Figure 15. Variation of (a) rotation and (b) transverse displacement along a Mindlin plate subjected to pure bending loading.

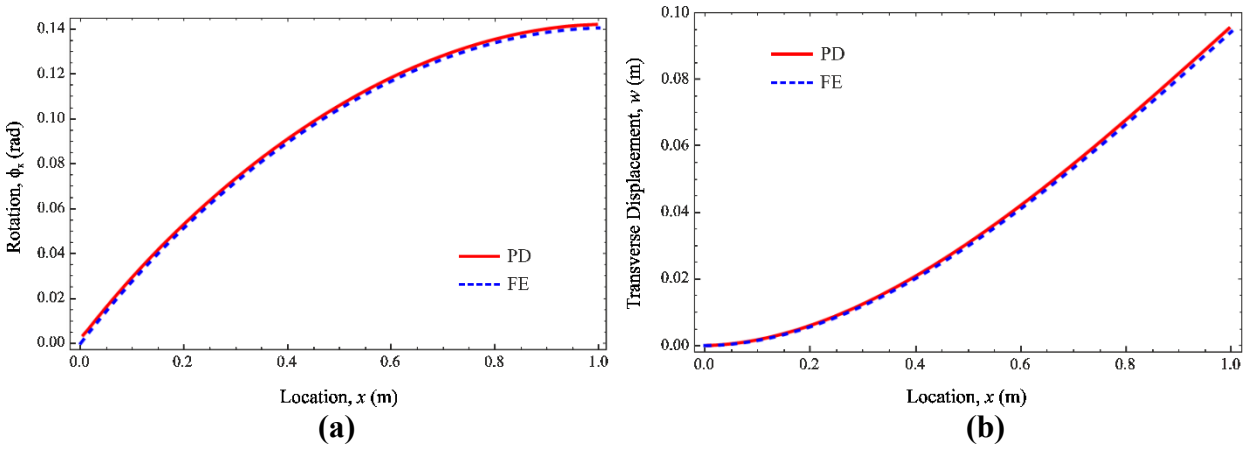

Figure 16. Variation of (a) rotation and (b) transverse displacement along a Mindlin plate subjected to transverse force loading.

7.3. Mindlin plate with central crack

Crack growth in a square plate with an initial central crack aligned with the *x*-axis, as shown in Fig. 17, is analyzed. The length and width of the plate are $L = W = 1\text{m}$ with a thickness of $h = 0.1\text{ m}$. Plate thickness to crack length ratio is $h/2a = 0.5$, which has the properties of a thick plate, where 2a is the initial crack length. The Young's modulus of the plate is specified as $E = 3.227\text{GPa}$ and the shear modulus is $G = 1.21\text{GPa}$. Only a single row of material (collocation) points in the thickness direction is necessary to discretize the domain. The distance between material points is $\Delta x = 2\times10^{-3}\text{ m}$. The horizon size is chosen as $\delta = 3.015\Delta x$.

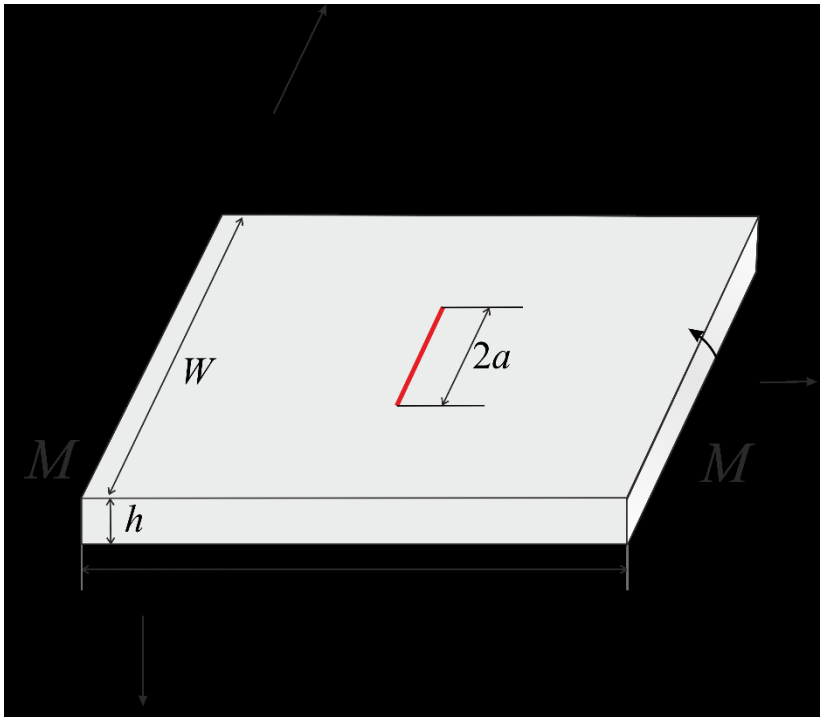

(a)

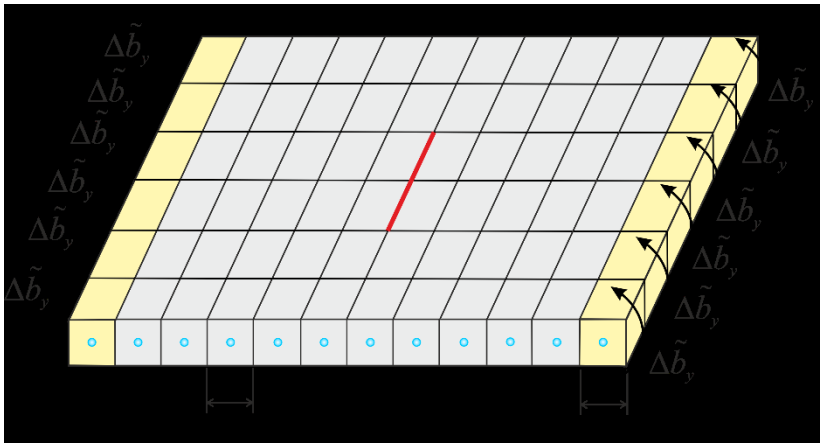

(b)

Figure 17. (a) Mindlin plate with a central crack subjected to pure bending loading and (b) its discretization.

The material is chosen as polymethyl-methacrylate (PMMA), which shows a brittle fracture behavior. Mode-I fracture toughness of this material is given as $1.33MPa\sqrt{m}$ (Ayatollahi and Aliha, 2009) and Mode-III fracture toughness is given as $7.684MPa\sqrt{m}$ (Farshad and Flueler, 1998). The critical energy release rates of mode-I and mode-III can be found from

$$G_{Ic}=\frac{K_{Ic}^2}{E} \quad \text{and} \quad G_{IIIc}=\frac{K_{IIIc}^2}{2G} \tag{47}$$

In order to show simple mode-I crack growth, a bending moment loading is applied through a single row of material points at the horizontal boundary regions of the plate. Small increments of resultant body loading of $\Delta\tilde{t}_y$ ___ N/m are induced in order to achieve stable crack growth. Under the applied uniform bending, the crack starts to grow at the end of nearly 66000 time steps, and as expected, it propagates towards the edges of the plate, as shown in Figs. 18a-d.

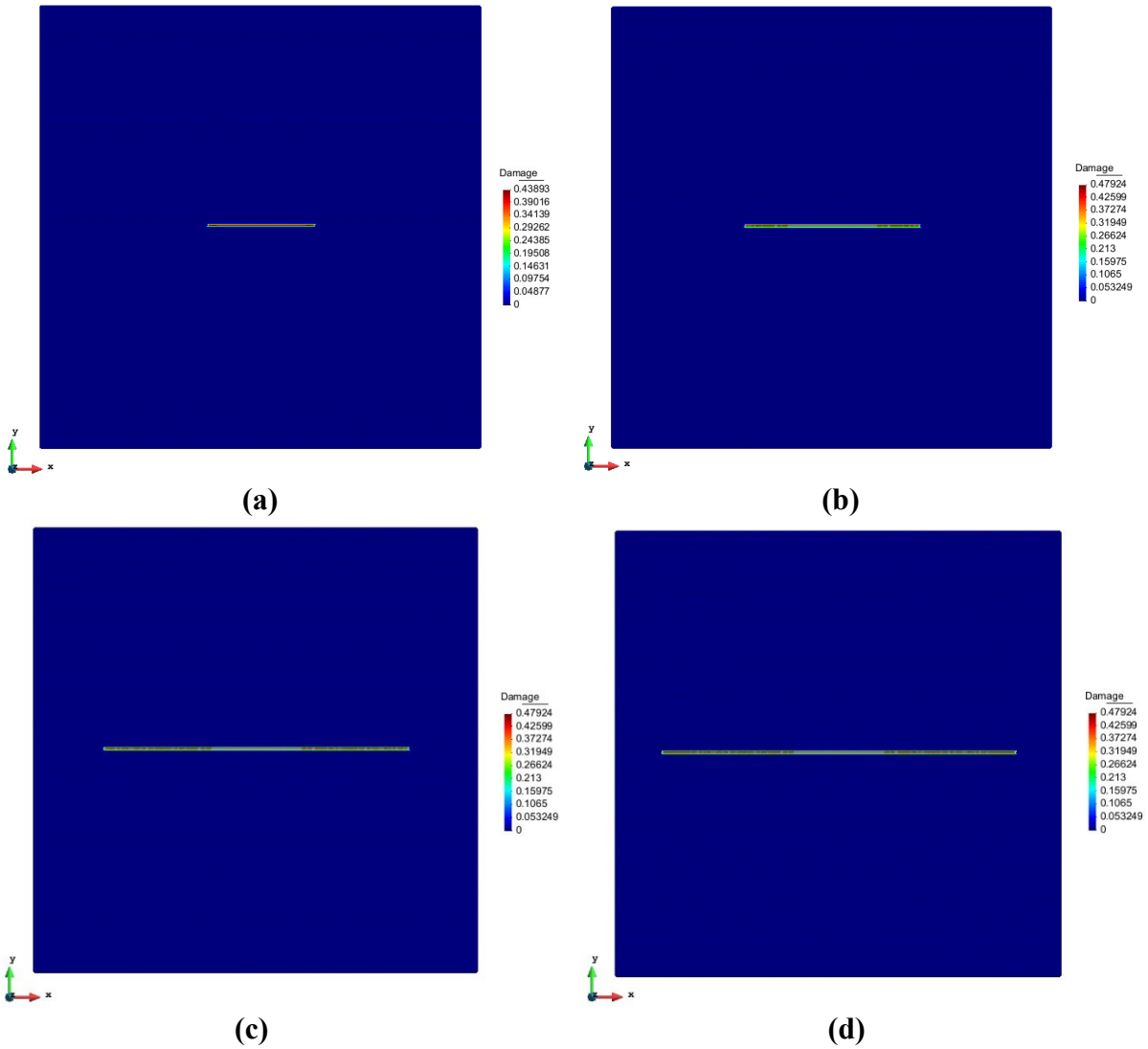

Figure 18. Crack evolution at (a) 66000th , (b) 67000th, (c) 68000th, and (d) 69000th time step.

8. Final remarks

This study presented the PD equations of motion for a Timoshenko beam and Mindlin plate. PD dispersion relationships were also obtained and it was observed that they are similar to the ones observed in real-materials, which cannot be predicted by using classical theory. After

establishing the validity of the PD predictions, the expressions for critical curvature and shear angle values in terms of mode-I and mode-III critical energy release rates of the material were also utilized to predict crack growth in a plate under pure bending.

References

A. Agwai, I. Guven and E. Madenci, 2011, "Predicting crack propagation with peridynamics: a comparative study," *Int. J. Fract.*, Vol. 171, pp. 65-78.

F. A. Amirkulova, 2011, "Dispersion Relations for Elastic Waves in Plates and Rods," M.Sc Thesis, Rutgers, The State University of New Jersey.

M. R. Ayatollahi and M. R. M. Aliha, 2009, "Analysis of a new specimen for mixed mode fracture tests on brittle materials," *Eng. Fract. Mech.*, Vol. 76, pp. 1563–1573.

A. C. Eringen, 1972, "Linear theory of nonlocal elasticity and dispersion of plane waves," *Int. J. Eng. Sci.*, Vol. 10 (5), pp. 425–435.

M. Farshad and P. Flueler, 1998, "Investigation of mode III fracture toughness using an anti-clastic plate bending method," *Eng. Fract. Mech.*, Vol. 60, pp. 597–603.

B. Kilic and E. Madenci, 2010, "An adaptive dynamic relaxation method for quasi-static simulations by using peridynamic theory," *Theor. Appl. Fract. Mec.*, Vol. 53, pp. 194-204.

E. Madenci and E. Oterkus, 2014, P*eridynamic Theory and Its Application*s, Springer, New York.

J. O'Grady and J. Foster, 2014a, "Peridynamic beams: A non-ordinary, state-based model," *Int. J. Solids Struct.*, Vol. 51, pp. 3177–3183.

J. O'Grady and J. Foster, 2014b, "Peridynamic plates and flat shells: A non-ordinary, state-based model," *Int. J. Solids Struct.*, Vol. 51, pp. 4572–4579.

M. de A. e S. Reis, 1978, "Wave Propagation in Elastic Beams and Rods," Ph.D. Dissertation, Massachusetts Institute of Technology.

S. A. Silling, 2000, "Reformulation of elasticity theory for discontinuities and long-range forces," *J. Mech. Phys. Solids*, Vol. 48, pp. 175–209.

S. A. Silling and E. Askari, 2005, "A meshfree method based on the peridynamic model of solid mechanics," *Comput. Struct.*, Vol. 83, pp. 1526–1535.

W. Soedel, 2004, *Vibrations of Shells and Plates (3rd ed.).* New York : Marcel Dekker.

M. Taylor and D. J. Steigmann, 2013, "A two-dimensional peridynamic model for thin plates," *Math. & Mech. of Solids*, pp. 1–13.

N. G. Stephen, 1997, "Mindlin Plate Theory: Best Shear Coefficient and Higher Spectra Validity," *J. Sound Vib.*, Vol. 202, pp. 539-553.

O. Weckner and S. A. Silling, 2011, "Determination of nonlocal constitutive equations from phonon dispersion relations," *Int. J. Mult. Comp. Eng.*, Vol. 9 (6), pp. 623–634.

Appendix A: PD material parameters

A.1 Timoshenko beam

As the horizon size approaches zero, PD equations must recover their classical counterparts. Therefore, the out-of-plane deflection and transverse shear angle at material point j can be expressed, using Taylor series expansion and disregarding higher order terms, as

$$\begin{aligned} w_{(j)} &= w_{(k)} + w_{(k),x}\xi_{(j)(k)}\,\mathrm{sgn}\left(x_{(j)} - x_{(k)}\right) + \frac{1}{2}w_{(k),xx}\xi_{(j)(k)}^2 \\ \phi_{(j)} &= \phi_{(k)} + \phi_{(k),x}\xi_{(j)(k)}\,\mathrm{sgn}\left(x_{(j)} - x_{(k)}\right) + \frac{1}{2}\phi_{(k),xx}\xi_{(j)(k)}^2 \end{aligned} \tag{A.1a,b}$$

Substituting from Eqs. (A.1a,b) into Eqs. (23a,b) and performing the algebraic manipulations lead to

$$\rho \ddot{\quad} \sum_{j=1}^{\infty}\left(w_{(k),xx} - \phi_{(k),x}\right)\xi_{(j)(k)}V_{(j)} + \hat{b}_{(k)} \tag{A.2a}$$

and

$$\frac{\rho I}{A}\ddot{\quad} \sum_{j=1}^{\infty}\phi_{(k),xx}\,\xi_{(j)(k)}V_{(j)} + c_s\sum_{j=1}^{\infty}\left(w_{(k),x} - \phi_{(k)} - \frac{1}{4}\phi_{(k),xx}\xi_{(j)(k)}^2\right)\xi_{(j)(k)}V_{(j)} + \tilde{\iota}_{(k)} \tag{A.2b}$$

Expressing the infinitesimal incremental volume, $V_{(j)} = A\Delta\xi_{(j)(k)}$, with $\Delta\xi_{(j)(k)}$ representing the spacing between two consecutive material points, and converting the summation to an integration as $\Delta\xi_{(j)(k)}$ approaches zero, i.e., $\Delta\xi_{(j)(k)} \to d\xi$, yield

$$\rho \ddot{\quad} \int_0^{\delta}\left(w_{,xx} - \phi_{,x}\right)\xi A d\xi + \hat{b} \tag{A.3a}$$

and

$$\frac{\rho I}{A}\ddot{\quad} \int_0^{\delta}\phi_{,xx}\xi\, A d\xi + c_s\int_0^{\delta}\left(w_{,x} - \phi - \frac{1}{4}\phi_{,xx}\xi^2\right)\xi A d\xi + \tilde{\iota} \tag{A.3b}$$

Performing the integrations results in

$$\rho \ddot{} \quad \frac{\delta^2}{2}\left(w_{,xx} - \phi_{,x}\right) + \hat{b} \tag{A.4a}$$

and

$$\frac{\rho I}{A} \ddot{} \quad \frac{\delta^2}{2}\left(c_b - c_s \frac{\delta^2}{8}\right)\phi_{,xx} + A\frac{\delta^2}{2} c_s \left(w_{,x} - \phi\right) + \tilde{\iota} \tag{A.4b}$$

Note that these PD equations of motion have the same form as those of the classical Timoshenko beam equations

$$\rho \ddot{} \quad w_{,xx} - \phi_{,x}\right) + \hat{b} \tag{A.5a}$$

and

$$\frac{\rho I}{A} \ddot{} \quad A \phi_{,xx} + k G\left(w_{,x} - \phi\right) + \tilde{\iota} \tag{A.5b}$$

where the shear correction factor, k , can be taken as $5/6$ for rectangular cross sections.
Finally, equating the coefficients of the independent variables in the PD equations of motion to those of the classical equations yields the relationships between the PD material constants, c_s and c_b, and the shear and Young's moduli, G and E, as

$$c_s = \frac{2kG}{A\delta^2} \quad \text{and} \quad c_b = \frac{2EI}{\delta^2 A^2} + \frac{1}{4}\frac{kG}{A} \tag{A.6a,b}$$

A.2 Mindlin plate

As the horizon size approaches zero, PD equations must recover their classical counterparts. Therefore, out-of-plane deflection and rotations at material point j can be expressed, using Taylor series expansion and disregarding higher order terms, as

$$\begin{aligned} w_{(j)} = w_{(k)} &+ w_{(k),x}\xi_{(j)(k)}\cos\theta + w_{(k),y}\xi_{(j)(k)}\sin\theta + \frac{1}{2}w_{(k),xx}\xi^2_{(j)(k)}\cos^2\theta \\ &+ w_{(k),xy}\xi^2_{(j)(k)}\cos\theta\sin\theta + \frac{1}{2}w_{(k),yy}\xi^2_{(j)(k)}\sin^2\theta \end{aligned} \tag{A.7a}$$

$$\begin{aligned} \phi_{\alpha(j)} = \phi_{\alpha(k)} &+ \phi_{\alpha(k),x}\xi_{(j)(k)}\cos\theta + \phi_{\alpha(k),y}\xi_{(j)(k)}\sin\theta + \frac{1}{2}\phi_{\alpha(k),xx}\xi^2_{(j)(k)}\cos^2\theta \\ &+ \phi_{\alpha(k),xy}\xi^2_{(j)(k)}\cos\theta\sin\theta + \frac{1}{2}\phi_{\alpha(k),yy}\xi^2_{(j)(k)}\sin^2\theta \end{aligned} \tag{A.7b}$$

Substituting from Eqs. (A.7a,b) into Eqs. (30a-c) and performing the algebraic manipulations lead to

$$\rho h\ddot{} \quad \frac{\pi}{2} \, h\frac{\delta^3}{3}\left(w_{,xx}+w_{,yy}-\phi_{x,x}-\phi_{y,y}\right)+\hat{b} \tag{A.8a}$$

$$\rho\frac{h^3}{12}\ddot{} \quad 16\,\delta^3\left(c_b\frac{2}{3}-c_s\frac{\delta^2}{10}\right)\left[3\phi_{x,xx}+\phi_{x,yy}+2\phi_{y,xy}\right]-\frac{\pi}{2}c_s h\frac{\delta^3}{3}\left(-w_{,x}+\phi_x\right)+\tilde{\iota}_x \tag{A.8b}$$

and

$$\rho\frac{h^3}{12}\ddot{} \quad 16\,\delta^3\left(c_b\frac{2}{3}-c_s\frac{\delta^2}{10}\right)\left[3\phi_{y,yy}+\phi_{y,xx}+2\phi_{x,xy}\right]-\frac{\pi}{2}c_s h\frac{\delta^3}{3}\left(-w_{,y}+\phi_y\right)+\tilde{\iota}_y \tag{A.8c}$$

The classical counterpart of the PD equations of motion for a Mindlin plate can be written as

$$\rho h\ddot{} \quad \left(w_{,xx}+w_{,yy}-\phi_{x,x}-\phi_{y,y}\right)+\hat{b} \tag{A.9a}$$

$$\frac{\rho h^3}{12}\ddot{} \quad \left[-\phi_{x,xx}+\frac{D}{2}(1-\nu)\phi_{x,yy}+\frac{D}{2}(1+\nu)\phi_{y,xy}\right]-k^2hG\left(\phi_x-w_{,x}\right)+\tilde{\iota}_x \tag{A.9b}$$

and

$$\frac{\rho h^3}{12}\ddot{} \quad \left[-\phi_{y,yy}+\frac{D}{2}(1-\nu)\phi_{y,xx}+\frac{D}{2}(1+\nu)\phi_{x,xy}\right]-k^2hG\left(\phi_y-w_{,y}\right)+\tilde{\iota}_y \tag{A.9c}$$

where k^2 is a correction coefficient that is introduced to account for the fact that the shear stresses are not constant over the thickness. The parameters *D* and G are the flexural rigidity and shear modulus, respectively, which are defined as

$$D=\frac{Eh^3}{12\left(1-\nu^2\right)} \quad \text{and} \quad G=\frac{E}{2(1+\nu)} \tag{A.10a,b}$$

The correction factor can be chosen based on the frequency of the lowest thickness shear mode as

$$k^2=\frac{\pi^2}{12} \tag{A.11}$$

Finally, equating equations of the peridynamic and classical theories reveals the relationships between the peridynamic material constants, c_s and c_b, and Young's modulus, *E*, as well as constraint on the value of the Poisson's ratio as

$$c_s = \frac{9E}{4\pi\delta^3}k^2 \quad \text{and} \quad c_b = \frac{E}{\pi\delta}\left(\frac{3h^2}{4\delta^2}+\frac{27}{80}k^2\right) \tag{A.12a,b}$$

and $\nu = 1/3$.

Appendix B: Surface corrections

B.1 Timoshenko beam

SED due to bending in the classical theory can be expressed as

$$W_b^{CM}\left(x_{(k)}\right) = \frac{1}{2}\left(\frac{EI}{A}\right)\kappa^2 \tag{B.1}$$

where $\kappa = \phi_{,x}$. Its counterpart in PD theory can be expressed in discretized form as

$$W_b^{PD}\left(x_{(k)}\right) = \frac{1}{2}\sum_{j=1}^{\infty}\frac{c_b}{2}\left(\kappa_{(k)(j)}\right)^2 \xi_{(j)(k)}V_{(j)} \tag{B.2}$$

Considering pure bending loading, the PD SED becomes

$$W_b^{PD}\left(x_{(k)}\right) = \frac{1}{2}\sum_{j=1}^{\infty}\frac{c_b}{2}\left(\kappa\right)^2 \xi_{(j)(k)}V_{(j)} \tag{B.3}$$

Hence, the surface correction factor for pure bending can be defined as

$$g_b\left(x_{(k)}\right) = \frac{W_b^{CM}\left(x_{(k)}\right)}{W_b^{PD}\left(x_{(k)}\right)} \tag{B.4}$$

On the other hand, SED due to transverse shear deformation in the classical theory can be written as

$$W_s^{CM}\left(x_{(k)}\right) = \frac{1}{2}Gk\left(\varphi\right)^2 \tag{B.5}$$

where $\varphi = w_{,x} - \phi$. Its counterpart in the PD theory can be expressed in discretized form as

$$W_s^{PD}\left(x_{(k)}\right) = \frac{1}{2}\sum_{j=1}^{\infty}\frac{c_s}{2}\left(\varphi_{(k)(j)}\right)^2 \xi_{(j)(k)}V_{(j)} \tag{B.6}$$

Considering pure shear loading along the *x*-direction, PD SED becomes

$$W_s^{PD}\left(x_{(k)}\right)=\frac{1}{2}\sum_{j=1}^{\infty}\frac{c_s}{2}\left(\varphi\right)^2\xi_{(j)(k)}V_{(j)} \tag{B.7}$$

Similar to pure bending, the correction factor for pure shear loading can be obtained as

$$g_s\left(x_{(k)}\right)=\frac{W_s^{CM}\left(x_{(k)}\right)}{W_s^{PD}\left(x_{(k)}\right)} \tag{B.8}$$

The surface correction factors for material point j and material point k can have different values; therefore, the surface correction factors for an interaction between material point j and material point k can be taken as their average

$$\bar{g}_b=\frac{g_b\left(x_{(k)}\right)+g_b\left(x_{(j)}\right)}{2} \tag{B.9a}$$

and

$$\bar{g}_s=\frac{g_s\left(x_{(k)}\right)+g_s\left(x_{(j)}\right)}{2} \tag{B.9b}$$

B.2 Mindlin plate

SED due to bending in the classical theory can be expressed as

$$W_b^{CM}\left(x_{(k)}\right)=\frac{1}{2}D\left(\kappa_x^2+2\nu\kappa_x\kappa_y+\kappa_y^2+\frac{1-\nu}{2}\kappa_{xy}^2\right) \tag{B.10}$$

where $\kappa_x=\phi_{\mathrm{x},x}$, $\kappa_y=\phi_{\mathrm{y},\mathrm{y}}$, and $\kappa_{xy}=\phi_{\mathrm{x},\mathrm{y}}+\phi_{\mathrm{y},\mathrm{x}}$. Its counterpart in the PD theory can be expressed in discretized form as

$$W_b^{PD}\left(x_{(k)}\right)=\frac{1}{2}\sum_{j=1}^{\infty}\frac{c_b}{2}\left(\kappa_{(k)(j)}\right)^2\xi_{(j)(k)}V_{(j)} \tag{B.11}$$

Considering pure bending loading along the *x*- and *y*-directions, i.e.

$$M_x=M_y\neq 0,\ M_{xy}=0 \tag{B.12}$$

results in curvatures

$$\kappa_x = \kappa_y \neq 0,\ \kappa_{xy} = 0 \tag{B.13}$$

The classical and PD SED for this loading condition become

$$W_b^{CM}\left(x_{(k)}\right) = \frac{1}{2} D\left(\kappa_x^2 + 2\nu\kappa_x\kappa_y + \kappa_y^2\right) \tag{B.14a}$$

and

$$W_b^{PD}\left(x_{(k)}\right) = \frac{1}{2}\sum_{j=1}^{\infty} \frac{c_b}{2}\left(\kappa_x \cos^2(\theta) + \kappa_y \sin^2(\theta)\right)^2 \xi_{(j)(k)} V_{(j)} \tag{B.14b}$$

Hence, the surface correction factor for pure bending can be defined as

$$g_b\left(x_{(k)}\right) = \frac{W_b^{CM}\left(x_{(k)}\right)}{W_b^{PD}\left(x_{(k)}\right)} \tag{B.15}$$

On the other hand, SED due to transverse shear deformation in the classical theory can be written as

$$W_s^{CM}\left(x_{(k)}\right) = \frac{1}{2} Gk^2 h\left(\left(\varphi_x\right)^2 + \left(\varphi_y\right)^2\right) \tag{B.16}$$

where $\varphi_x = w_{,x} - \phi_x$ and $\varphi_y = w_{,\mathrm{y}} - \phi_y$. Its counterpart in the PD theory can be expressed in discretized form as

$$W_s^{PD}\left(x_{(k)}\right) = \frac{1}{2}\sum_{j=1}^{\infty} \frac{c_s}{2}\left(\varphi_{(k)(j)}\right)^2 \xi_{(j)(k)} V_{(j)} \tag{B.17}$$

Applying pure shear loading along the *x*-direction, i.e.

$$Q_x \neq 0 \ \text{ and } \ Q_y = 0 \tag{B.18}$$

results in shear angles

$$\varphi_x \neq 0 \text{ and } \varphi_y = 0\,. \tag{B.19}$$

Classical and PD SED for this loading condition become

$$W_s^{CM}\left(x_{(k)}\right) = \frac{1}{2} Gk^2 h\left(\varphi_x\right)^2 \tag{B.20a}$$

and

$$W_s^{PD}\left(x_{(k)}\right)=\frac{1}{2}\sum_{j=1}^{\infty}\frac{c_s}{2}\left(\varphi_x\cos\left(\theta\right)\right)^2\xi_{(j)(k)}V_{(j)} \tag{B.20b}$$

Similar results can also be obtained for pure shear loading along the *y*-direction as

$$W_s^{CM}\left(x_{(k)}\right)=\frac{1}{2}Gk^2h\left(\varphi_y\right)^2 \tag{B.21a}$$

and

$$W_s^{PD}\left(x_{(k)}\right)=\frac{1}{2}\sum_{j=1}^{\infty}\frac{c_s}{2}\left(\varphi_y\sin\left(\theta\right)\right)^2\xi_{(j)(k)}V_{(j)} \tag{B.21b}$$

Similar to pure bending, the correction factor for pure shear loading can be obtained as

$$g_s\left(x_{(k)}\right)=\frac{W_s^{CM}\left(x_{(k)}\right)}{W_s^{PD}\left(x_{(k)}\right)} \tag{B.22}$$

The surface correction factors for material point j and material point k can have different values; therefore, the surface correction factors for an interaction between material point j and material point k can be taken as their average

$$\bar{g}_b=\frac{g_b\left(x_{(k)}\right)+g_b\left(x_{(j)}\right)}{2} \tag{B.23a}$$

and

$$\bar{g}_s=\frac{g_s\left(x_{(k)}\right)+g_s\left(x_{(j)}\right)}{2} \tag{B.23b}$$

Appendix C: Dispersion relations

C.1 Timoshenko beam

The terms appearing in Eq. (33) are defined as

$$B_1 = \int_0^{\delta} \left(1 + \cos\left(\kappa\xi\right)\right) \xi d\xi \tag{C.1a}$$

$$B_2 = \int_0^{\delta} \frac{\left(1 - \cos\left(\kappa\xi\right)\right)}{\xi} d\xi \tag{C.1b}$$

and

$$B_3 = \int_0^{\delta} i \sin\left(\kappa\xi\right) d\xi \tag{C.1c}$$

As suggested by Silling (2000), in the limit of long wavelength (or small κ), these integrals can be analytically evaluated by considering the first three terms of the Taylor series expansion of the cosine and sine functions

$$\cos(\kappa\xi) = 1 - \frac{\left(\kappa\xi\right)^2}{2!} + \frac{\left(\kappa\xi\right)^4}{4!} - \ldots \tag{C.2a}$$

and

$$\sin(\kappa\xi) = \kappa\xi - \frac{\left(\kappa\xi\right)^3}{3!} + \frac{\left(\kappa\xi\right)^5}{5!} - \ldots \tag{C.2b}$$

With the evaluation of these integrals and considering the PD material parameters, the determinant from Eq. (33) can be expressed as

$$\begin{aligned} &\Omega_{pd}^4 - \Omega_{pd}^2 \left(2\left(1+\nu\right)\zeta^2 + k\zeta^2 + mk - \frac{\left(1+\nu\right)\zeta^4}{12t^2} - \frac{k\zeta^4}{24t^2} + \frac{mk\zeta^4}{576t^4} \right) + \frac{k\left(1+\nu\right)\zeta^8}{288t^4} + \frac{mk^2\zeta^8}{2560t^6} \\ &- \frac{k\left(1+\nu\right)\zeta^6}{6t^2} - \frac{31mk^2\zeta^6}{2880t^4} + 2k\left(1+\nu\right)\zeta^4 - \frac{mk^2\zeta^{10}}{129600t^8} + \frac{mk^2\zeta^4}{8t^2} = 0 \end{aligned} \tag{C.3}$$

in which ν is the Poisson's ratio. The nondimensional wave frequency and wave number, Ω_{pd} and ζ, respectively, are defined as

$$\Omega_{pd} = \frac{\omega h}{\upsilon_s} \text{ and } \zeta = \kappa h \tag{C.4a,b}$$

The non-dimensional geometric parameters, m and t, are defined as

$$m = \frac{Ah^2}{I} \text{ and } t = \frac{h}{\delta} \tag{C5.a,b}$$

Disregarding the higher order terms of the horizon simplifies the wave dispersion relation for long wavelength limit (or small ζ) as

$$\Omega_{pd}^4 - \Omega_{pd}^2\left(2(1+\nu)\zeta^2 + k\zeta^2 + mk\right) + 2k(1+\nu)\zeta^4 = 0 \tag{C.6}$$

As expected, this equation recovers the nondimensional wave dispersion relation in the classical theory (CT) (Amirkulova, 2011) for a long wavelength limit. It leads to four different values for wave frequency, which represent two waves traveling to the right and two waves traveling to the left of the beam. Therefore, there are two distinct modes that can propagate in a Timoshenko beam (Reis, 1978). The first mode yields zero frequency ($\Omega = 0$) when the wave number is equal to zero ($\zeta = 0$)

$$\Omega_{ccm} = \Omega_{pd} = \sqrt{\zeta^2(1+\nu) + \frac{\zeta^2 k}{2} + \frac{km}{2} - \sqrt{\left(\zeta^2(1+\nu) + \frac{\zeta^2 k}{2} + \frac{km}{2}\right)^2 - \zeta^4\left(2k(1+\nu)\right)}} \tag{C.7}$$

and the second mode can be expressed as

$$\Omega_{ccm} = \Omega_{pd} = \sqrt{\zeta^2(1+\nu) + \frac{\zeta^2 k}{2} + \frac{km}{2} + \sqrt{\left(\zeta^2(1+\nu) + \frac{\zeta^2 k}{2} + \frac{km}{2}\right)^2 - \zeta^4\left(2k(1+\nu)\right)}} \tag{C.8}$$

The wave dispersion relations for long wavelength limit are shown in Figs. C.1 and C.2 for the specified values of $E = 200$ GPa, $\rho = 7850$ kg/m^3, $k = 5/6$, $h = 10^{-7}$ m, $\nu = 0.3$, and horizon size, $\delta = 10^{-8}$ m.

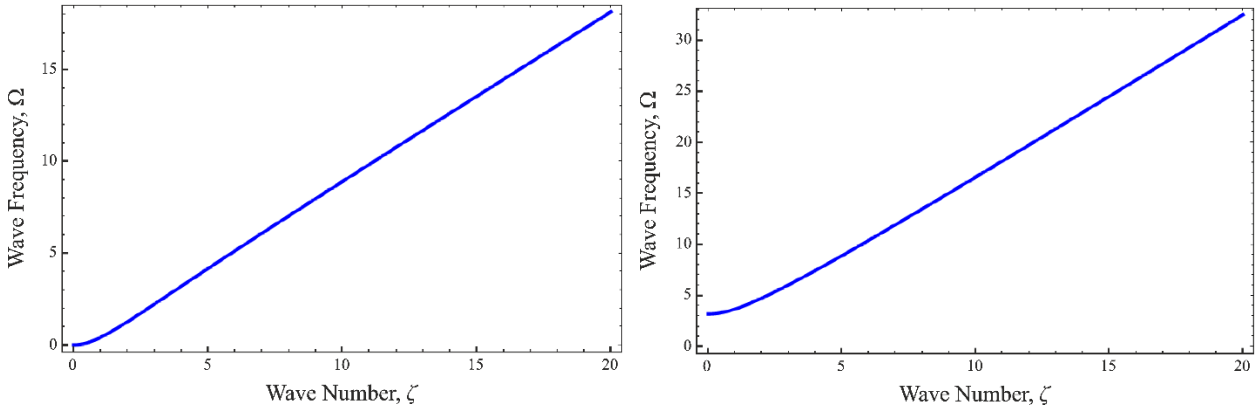

Figure C.1. Classical wave frequency dispersion for the first and second modes (combine these plots)

Note that the wave number of the second mode is real for $\Omega \geq 3.16$. This indicates that the first mode is a propagating mode for any wave frequency, while the second mode only propagates for wave frequencies $\Omega \geq 3.16$ and is exponentially attenuated for $\Omega < 3.16$, as discussed by Reis (1978). Therefore, $\Omega = 3.16$ is the cut-off frequency for the second mode.

The variations of nondimensional phase speed, $\upsilon = \Omega / \left(\zeta \sqrt{k} \right)$ and $\upsilon = \Omega / \left(\zeta \sqrt{E/G} \right)$, as a function of the wave number are shown in Fig. C.2 for the first and second modes.

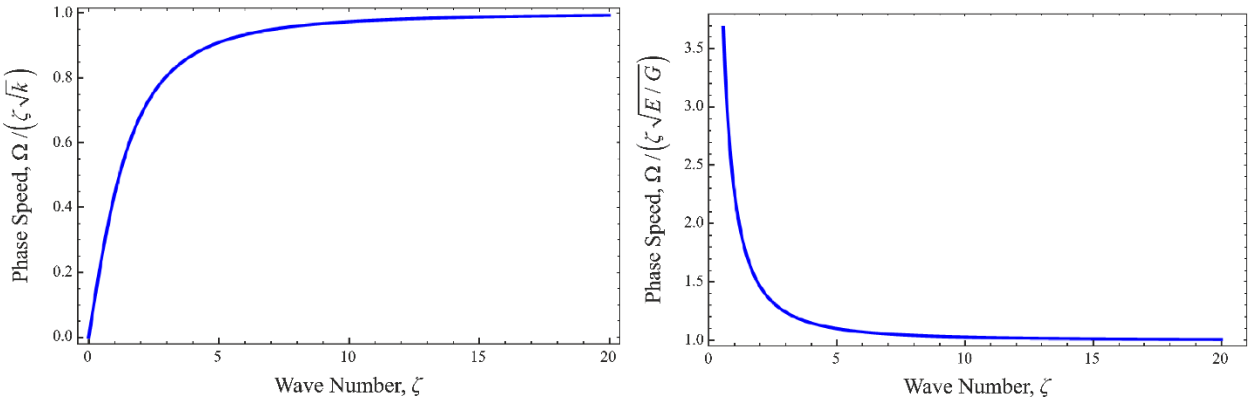

Figure C.2. Classical wave speed dispersion for the first and second modes

The phase speed, $\upsilon = \Omega / \left(\zeta \sqrt{k} \right)$ or $\upsilon = \Omega / \left(\zeta \sqrt{E/G} \right)$, converges to unity as the wave number, ζ, increases. Hence, the phase speed for the first mode, $\upsilon = \Omega / \left(\zeta \sqrt{k} \right)$, converges to the shear wave speed, υ_s, of the CT, since

$$\upsilon = \frac{\omega}{\kappa} \quad \text{and} \quad \frac{\Omega}{\zeta \sqrt{k}} = \frac{\upsilon}{\upsilon_s \sqrt{k}} \tag{C.9}$$

Moreover, the phase speed for the second mode, $\upsilon = \Omega / \left(\zeta \sqrt{E/G} \right)$, converges to the compressional wave speed, υ_c, of the CT, since

$$\frac{\Omega}{\zeta \sqrt{\frac{E}{G}}} = \frac{\upsilon}{\upsilon_c} \tag{C.10}$$

C.2 Mindlin plate

The terms appearing in Eq. (35) are defined as

$$M_1 = \int_0^{2\pi}\int_0^{\delta} \frac{e^{i\kappa\xi\cos(\theta)}-1}{\xi} dV \tag{C.11a}$$

$$M_2 = \int_0^{2\pi}\int_0^{\delta} \frac{e^{i\kappa\xi\cos(\theta)}+1}{2}\cos(\theta)\, dV \tag{C.11b}$$

$$M_3 = \int_0^{2\pi}\int_0^{\delta} \frac{e^{i\kappa\xi\cos(\theta)}+1}{2}\sin(\theta)\, dV \tag{C.11c}$$

$$M_4 = \int_0^{2\pi}\int_0^{\delta} \frac{e^{i\kappa\xi\cos(\theta)}-1}{\xi}\cos^2(\theta) dV \tag{C.11d}$$

$$M_5 = \int_0^{2\pi}\int_0^{\delta} \frac{e^{i\kappa\xi\cos(\theta)}-1}{\xi}\sin(\theta)\cos(\theta) dV \tag{C.11e}$$

$$M_6 = \int_0^{2\pi}\int_0^{\delta} \left(e^{i\kappa\xi\cos(\theta)}-1\right)\cos(\theta) dV \tag{C.11f}$$

$$M_7 = \int_0^{2\pi}\int_0^{\delta} \frac{e^{i\kappa\xi\cos(\theta)}+1}{2}\xi\cos^2(\theta) dV \tag{C.11g}$$

$$M_8 = \int_0^{2\pi}\int_0^{\delta} \frac{e^{i\kappa\xi\cos(\theta)}+1}{2}\xi\sin(\theta)\cos(\theta) dV \tag{C.11h}$$

$$M_9 = \int_0^{2\pi}\int_0^{\delta} \frac{e^{i\kappa\xi\cos(\theta)}-1}{\xi}\sin^2(\theta) dV \tag{C.11i}$$

$$M_{10} = \int_0^{2\pi}\int_0^{\delta} \left(e^{i\kappa\xi\cos(\theta)}-1\right)\sin(\theta) dV \tag{C.11j}$$

$$M_{11} = \int_0^{2\pi}\int_0^{\delta} \frac{e^{i\kappa\xi\cos(\theta)}+1}{2}\xi\sin^2(\theta) dV \tag{C.11k}$$

in which dV denotes the infinitesimal volume of a material point, which can be written in cylindrical coordinates as $dV = h\xi d\xi d\theta$. Evaluation of these integrals yields Bessel functions of the first kind, $J_0(\kappa\delta)$ and $J_1(\kappa\delta)$, and Struve functions, $H_0(\kappa\delta)$ and $H_1(\kappa\delta)$.

As indicated by Silling (2000), in the limit of a long wavelength (Γ) or for a very small wave number ($\kappa \to 0$), the integrals in Eqs. (C.11a-k) can be simplified by using the first three terms of the Taylor series expansion for cosine and sine functions

$$\cos\left(\kappa\xi\cos(\theta)\right) = 1 - \frac{\left(\kappa\xi\cos(\theta)\right)^2}{2!} + \frac{\left(\kappa\xi\cos(\theta)\right)^4}{4!} - \ldots \tag{C.12a}$$

and

$$\sin(\kappa\xi\cos(\theta)) = \kappa\xi\cos(\theta) - \frac{(\kappa\xi\cos(\theta))^3}{3!} + \frac{(\kappa\xi\cos(\theta))^5}{5!} - \ldots \qquad \text{(C.12b)}$$

Substituting the relationships given in Eqs. (C.12a,b) into integrations given in Eqs. (C.11a-k) and solving the determinant equation given in Eq. (35), while ignoring higher order terms of horizon size, yield the dispersion relationship for a long wavelength limit in the PD theory

$$\begin{vmatrix} -k^2Gh\kappa^2 + \rho h\omega^2 & -k^2Ghi\kappa & 0 \\ k^2Ghi\kappa & -D\kappa^2 - k^2Gh + \frac{\rho h^3}{12}\omega^2 & 0 \\ 0 & 0 & -\frac{D}{2}(1-\nu)\kappa^2 - k^2Gh + \frac{\rho h^3}{12}\omega^2 \end{vmatrix} = 0 \qquad \text{(C.13)}$$

with the constraint on Poisson's ratio ($\nu = 1/3$).

This relationship is equivalent to the dispersion relationship obtained from the classical theory (CT). Moreover, roots of Eq. (C.13) correspond to three different natural frequencies. Soedel (2004) explained that the lowest of these frequencies is the one that the transverse deflection mode dominates and other two are considered as shear modes.

Shown in Fig. C.3 are the nondimensionalized phase speed (υ/υ_s) dispersion relationships with the change of wave number (h/Γ) for three different wave modes for the long wavelength limit while considering the following properties of a plate $k^2 = 5/(6-\nu)$ and $\nu = 1/3$.

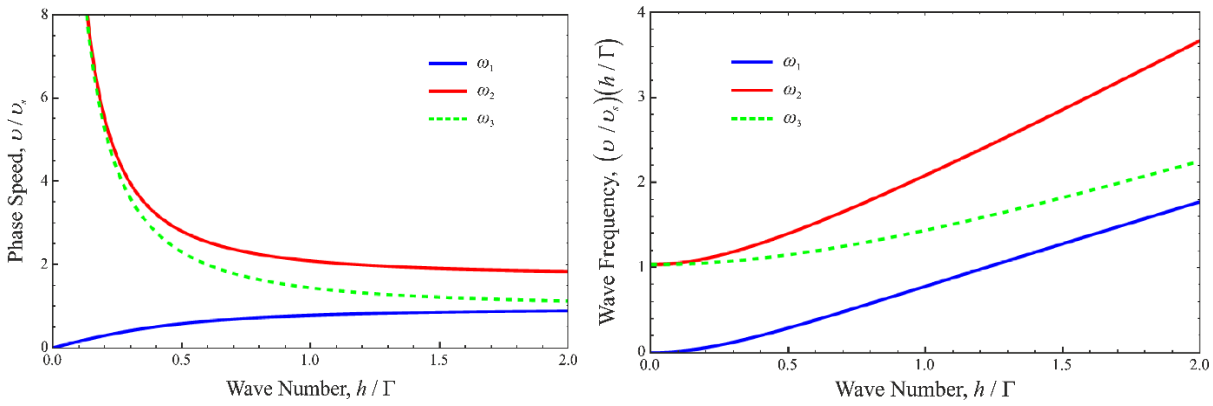

Figure C.3. Classical phase speed dispersions and wave frequency dispersions.

Variations similar to those in Fig. C.3 and comparisons with Rayleigh-Lamb waves, which have the property of waves in a plate with infinite extent, can be seen in Stephen (1997). Also, in Stephen (1997), ω_1 is named as the lowest flexural mode, ω_2 as the thickness-shear mode, and

ω_3 as the thickness-twist mode. In Fig. C.3, when the wave number (h/Γ) reaches the value of two, which means the wave length is now comparable with the thickness of a plate, all the phase speeds become flat.

Figure C.3 shows the nondimensionalized wave frequency ($\left(\upsilon/\upsilon_s\right)\left(h/\Gamma\right)$) dispersions with the change of wave number (h/Γ) for three wave modes of the CT or for the PD theory in the long wavelength limit.